originally reported in human AML. Therefore, in order to identify a cellular target for *PML-RARA* that effectively develops APL, *PML-RARA* was transduced into fractionated cells: $CD34^+/CD38^-$, $CD34^+/CD38^+$ and $CD34^-/CD33^+$ cells from the cord blood (**Figures 6A and 6B**). The transduction efficiency, as evaluated by EGFP expression, ranged from 1.9% to 5.0% (median: 3.53%, n = 6) in $CD34^+/CD38^-$ cells, 4.5% to 10.6% (median: 10.07%, n = 6) in $CD34^+/CD38^+$ cells and 19.1% to 22.1% (median: 20.63%, n = 4) in $CD34^-/CD33^+$ cells. Because the $CD34^+$ fraction from human cord blood possessed a higher proportion of $CD34^+/CD38^+$ (74.5% to 94.2%) than that of $CD34^+/CD38^-$ cells, the presumed absolute number of *PML-RARA* transplanted cells was higher in $CD34^+/CD38^+$ cells than in $CD34^+/CD38^-$ cells (3,430 to 31,800 cells vs 140 to 450 cells per mouse; 22,900 to 27,700 $CD34^-/CD33^+$ cells). One hundred unfractionated human $CD34^+$ cells, including both $CD34^+/CD38^-$ and $CD34^+/CD38^+$ cells, were engrafted with multilineage differentiation in our previous study [10], thus suggesting that the transplanted cell numbers were adequate for engraftment in the NOG mice. The induction of *PML-RARA* in $CD34^+/CD38^+$ cells reduced the colony formation capacity and favored the formation of myeloid colonies, as seen in $CD34^+$ cells (**Figures 1B and 1C**). On the other hand, the induction of *PML-RARA* in $CD34^+/CD38^-$ cells generated very few colonies in comparison to the MIGR1 control vector-infected $CD34^+/CD38^-$ cells (**Figures 6C and 6D**). Consistent with the results, the induced APL cells were detected mostly in the mice transplanted with $CD34^+/CD38^+$ cells (median, 16.4% in the whole bone marrow cells) (**Figure 6E**). These findings suggest that $CD34^+/CD38^+$ progenitors proliferate and survive more efficiently than $CD34^+/CD38^-$ cells *in vitro* and trigger APL *in vivo* by inducing *PML-RARA*.

Human common myeloid progenitors develop into APL by inducing *PML-RARA* among $CD34^+/CD38^+$ progenitors

In order to identify the detailed target fraction in $CD34^+/CD38^+$ cells that generates APL with *PML-RARA*, the $CD34^+/CD38^+$ cells were then divided into three fractions based on their expression of CD123 and CD45RA; CMP, GMP and MEP (**Figure 6F**). The retroviral transduction efficiencies of *PML-RARA* into CMP, GMP and MEP were 6.0% to 15.2% (median: 6.6%, n = 9), 3.3% to 8.8% (median: 7.1%, n = 8), and 7.8% to 24.6% (median: 8.5%, n = 7) (**Figure 6G**), and the presumed absolute numbers of *PML-RARA* transduced cells in CMP, GMP and MEP utilized for the transplantation were 5,850 to 15,200, 830 to 4,250, and 1,150 to 2,550 cells per mouse, respectively, which were deduced to directly reflect their proportion in the human cord blood. The frequency of induced APL cells in whole bone marrow cells from transplanted NOG mice was higher when using CMP (median, 25.2%) than GMP and MEP (median, 0.15% and 0.01%, respectively) (**Figure 6H**).

Taken together, these findings obtained using our humanized *in vivo* APL model demonstrate that CMP are a target fraction for *PML-RARA* in the development of APL.

Discussion

Our present study revealed that a humanized APL model was successfully established by transplantation of human $CD34^+$ cord blood transduced with *PML-RARA* into immunodeficient mice. Using this model, we demonstrated that the CMP develop into APL by transducing *PML-RARA* whereas the resultant $CD34^-$ APL cells had the ability to maintain the tumor. Our system improves in the following points: The induced APL cells were detected in all of the mice within 150 days if more than 3,000 human $CD34^+$ cells infected with *PML-RARA* were transplanted into NOG mice. The resultant leukemia well recapitulated the human disease phenotypically, genetically and functionally, including the presence of Auer rods and Faggot cells, and the expression pattern of cellular surface markers and transcripts, as well as ATRA sensitivity and low leukemia transplantability. These findings demonstrated that this humanized *in vivo* model is suitable for prospectively analyzing the process of APL development in humans.

The cellular subset from which the APL originates is still controversial. Several lines of evidence using *in vivo* experiments have suggested that APL arises in the committed myeloid progenitors, whereas several clinical observations using FISH and RT-PCR analyses suggest that APL arises in earlier progenitors [4]. A recent report using conditional knock-in mice showed that the induction of *PML-RARA* led to dominant proliferation in a stem cell compartment with multilineage potential, but did not result in myeloproliferation, as if the stem cell compartment would not support leukemogenesis in this model [34,35]. Our *in vitro* and *in vivo* findings are compatible with the previous findings which showed that the generation of *PML-RARA* transgenic mice was only possible by expressing *PML-RARA* in early myeloid cells using the human cathepsin G (hCG) and MRP8 promoters, not the promoters of β-actin, a housekeeping gene, and CD11b which is expressed at a later stage of myeloid differentiation [36].

The leukemogenic function of PML-RARα may require subtle myeloid differentiation, as seen in CMP in the present study; PML-RARα has been reported to possess the inhibitory or toxic effects on the cellular survival, senescence or apoptosis [18,37,38]. CMP are still immature enough to easily acquire stemness and are already committed to the myeloid lineage, which may allow *PML-RARA* to dysregulate RARα-dependent myelopoiesis, rather than hematopoietic stem cells, in agreement with the fact that *RARA* is implicated in the regulation of myelopoiesis, including both early stage and terminal differentiation. In this scenario, the expression of *PML-RARA* would induce differentiation of CMP to promyelocytes, but inhibit their terminal differentiation at the same time [19,39,40]. Therefore, if the CMP expressing *PML-RARA* acquires stemness, this can result in the development of APL. Our findings showed no engraftment of $CD34^+/CD38^-$ cells with *PML-RARA* transduction *in vivo*, although their leukemogenic activity cannot be denied, as fewer cells were transplanted in comparison to the $CD34^+/CD38^+$ cells. Further analyses are required to evaluate whether $CD34^+/CD38^-$ cells possess the ability to cause APL.

Xenograft models using immunodeficient mice are at present the only method for evaluating the maintenance of human leukemia as LIC. The induced APL generated in the NOG mice had a low engraftment efficiency; however, this biological feature well-reproduced the properties of APL cells found in human patients [3,12]. It is possible that the difficulty associated with engrafting APL cells, both primary samples and induced APL cells obtained from cord blood, into NOG mice may depend on the different preferences of human hematopoietic cells between humans and mice. The reconstitution of the human hematopoietic system in NOG mice is achieved with the dominant engraftment of B-cells, in comparison to the myeloid lineage cells [10]. This technical feature may affect the engraftment of each of the transplanted cellular subsets in our study. The slow progressive myeloid tumor cells, such as those involved in myelodysplastic syndromes and chronic myeloid leukemia in the chronic phase, were shown to be difficult to engraft in NOD/SCID-β2-

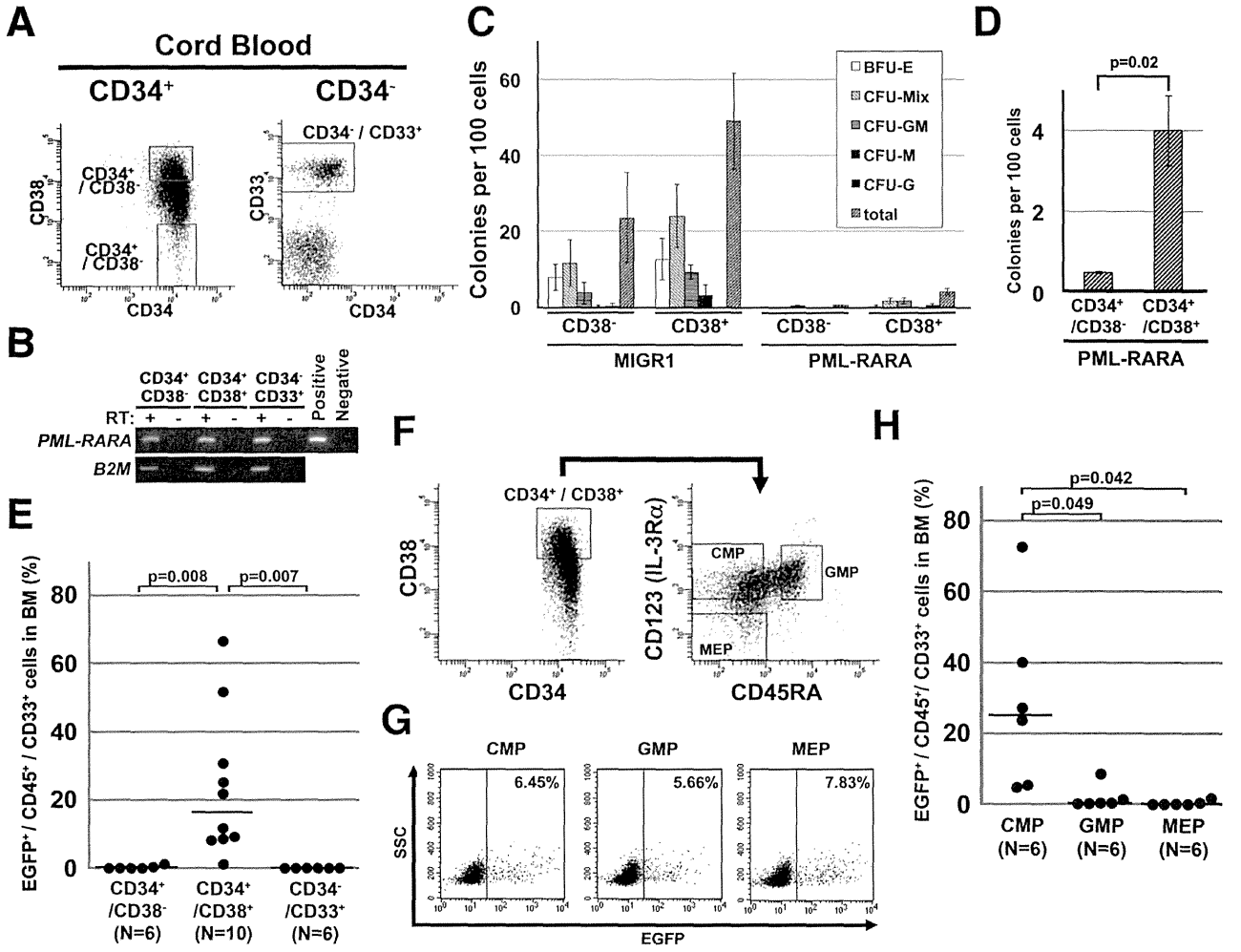

Figure 6. *PML-RARA* targeted human common myeloid progenitors for APL leukemogenesis. (**A**) The sorting strategy for $CD34^+/CD38^-$, $CD34^+/CD38^+$ and $CD34^-/CD33^+$ cells. Human cord blood was first separated into $CD34^+$ and $CD34^-$ cells by magnetic beads, and then sorted into three fractions by a FACS vantage instrument. (**B**) The expression of *PML-RARA* mRNA in each of the fractions after retroviral transfection. *B2M, beta 2 microglobulin.* The *PML-RARA* expression vector was used as a positive control for the *PML-RARA* analysis. (**C**) A colony-forming assay using *PML-RARA*-transduced $CD34^+/CD38^+$ and $CD34^+/CD38^-$ cells. The average of three independent experiments is shown. The data represent the means ± SD. (**D**) The total numbers of colonies of *PML-RARA*-transduced $CD34^+/CD38^+$ and $CD34^+/CD38^-$ cells shown in (C) are highlighted. The data represent the means ± SD (n = 3). (**E**) The development of the induced APL from $CD34^+/CD38^+$ cells in NOG mice. Each sorted fraction from human cord blood, as seen in (A), was retrovirally transduced with *PML-RARA* and transplanted into irradiated NOG mice. The percentages were determined by the frequency of $EGFP^+/CD45^+/CD33^+$ cells at 16 to 20 weeks after transplantation. Each dot represents a single mouse. The horizontal line represents the median value. (**F**) The sorting strategy for common myeloid progenitors (CMP), granulocyte-monocytic progenitors (GMP), and megakaryocyte-erythrocyte progenitors (MEP). Human cord blood was separated into $CD34^+$ cells by magnetic beads, $CD34^+/CD38^+$ cells were sorted out, and were finally divided into CMP, GMP and MEP by the FACS vantage instrument. (**G**) The transduction efficiency of *PML-RARA* in CMP, GMP and MEP. Representative data are shown. (**H**) The development of the induced APL from the human hematopoietic progenitors in NOG mice. Each sorted progenitor fraction from human cord blood, as seen in (F), was retrovirally transduced with *PML-RARA* and transplanted into irradiated NOG mice. The percentages were determined by the frequency of $EGFP^+/CD45^+/CD33^+$ cells at 16 to 20 weeks after transplantation. Each dot represents a single mouse. The horizontal line represents the median value.
doi:10.1371/journal.pone.0111082.g006

microglobulin-deficient or NOG mice (the previous reports [41–43] and our unpublished data), suggesting that the engraftment failure did not always indicate a lack of leukemogenecity of the transplanted cells. Therefore, our study confirmed the leukemogenic activity of the $CD34^-$ induced APL fraction, although it was not strong. These results are consistent with the previous *in vivo* reports which described the some primary $CD34^+/CD38^+$ and $CD34^-$ AML cells could function as LIC *in vivo* [44,45].

In conclusion, we demonstrated that the induction of *PML-RARA* targeted human $CD34^+$ cells, including CMP, and led to their ability to cause APL, and that $CD34^-$ APL cells have the capability of maintaining the disease. These findings suggest that it is not necessary that LIC are always consistent with a cellular fraction where leukemia-inducing events occur. Tumor-specific oncogenes, such as *PML-RARA*, effectively function to form tumors with specific characteristics in specific hierarchal stages of myelopoiesis. This model differs from the conventional hierarchal system of AML, in which LIC possess an immature phenotype as seen in hematopoietic stem cells. Since AML is a group of heterogeneous diseases with various causal genetic abnormalities,

the present findings will be helpful for the analysis of leukemogenesis in other types of AML which display differentiated leukemic blasts.

Supporting Information

Figure S1 The detection of *PML-RARA* expression in $CD34^+$ cells transduced with *PML-RARA* and their descendent colonies by qualitative RT-PCR. RT, reverse transcription.
(TIF)

Figure S2 Fluorescent images of the colonies derived from the $EGFP^+$ and $EGFP^-$ fractions of the $CD34^+$ cells transduced with *PML-RARA*.
(TIF)

Figure S3 The results of a quantitative analysis of the *PML-RARA* expression in the $CD34^+$ cells 48 hours after *PML-RARA* transduction, the differentiated cells from the resultant colonies and the induced APL cells. There were significant differences in the comparison of the expression level of *PML-RARA*. * indicates p values <0.05.
(TIF)

Figure S4 The heat map of the microarray analysis using the 3,439 probes (3,278 genes) that were differentially expressed in the induced APL (n = 3) and the AML other than APL (n = 62). The gene set separated the induced and human primary APL from the cases of AML other than APL. Red triangles (n = 2 from the total of 16 APL cases) show the clinical APL samples whose microarray data were obtained in this study.
(TIF)

Figure S5 The heat map of the microarray analysis performed using the gene set composed of 573 probes (547 genes), which were specifically expressed in the induced APL in comparison to cases of AML other than APL and normal promyelocytes. The gene set clearly clustered the malignant promyelocytes, such as the induced and human primary APL, apart from the normal promyelocytes. Red triangles (n = 2 of a total 16 APL cases) show the clinical APL samples whose microarray data were obtained in this study.
(TIF)

Table S1 The sequences of the PCR primers and probes.
(XLSX)

Table S2 KEGG pathway analysis with the gene sets aberrantly expressed in the induced APL.
(XLSX)

Table S3 The gene set apllied in Figure S5 (573 probes).
(XLSX)

Table S4 The integration sites of PML-RARA in the induced APL cells.
(XLSX)

Acknowledgments

We thank Dr. Warren S. Pear (University of Pennsylvania) for providing the MIGR1 retroviral vector, Dr. Toshio Kitamura (The University of Tokyo) for providing the PLAT-gp packaging cells, Dr. Guilherme Santos (Beth Israel Deaconess Medical Center, Harvard Medical School) for his valuable suggestions and comments, and Tomoko Uno and Tomomi Takanashi (Tokai University School of Medicine) for their expert technical assistance.

Author Contributions

Conceived and designed the experiments: H. Matsushita KA. Performed the experiments: H. Matsushita TY YS YN YM H. Matsuzawa TS AD H. Miyachi. Analyzed the data: H. Matsushita TY MT HH. Contributed reagents/materials/analysis tools: MO MI PPP. Wrote the paper: H. Matsushita TY KA.

References

1. Lowenberg B (2008) Acute myeloid leukemia: the challenge of capturing disease variety. Hematology Am Soc Hematol Educ Program: 1–11.
2. Lapidot T, Sirard C, Vormoor J, Murdoch B, Hoang T, et al. (1994) A cell initiating human acute myeloid leukaemia after transplantation into SCID mice. Nature 367: 645–648.
3. Bonnet D, Dick JE (1997) Human acute myeloid leukemia is organized as a hierarchy that originates from a primitive hematopoietic cell. Nat Med 3: 730–737.
4. Grimwade D, Enver T (2004) Acute promyelocytic leukemia: where does it stem from? Leukemia 18: 375–384.
5. Hope KJ, Jin L, Dick JE (2004) Acute myeloid leukemia originates from a hierarchy of leukemic stem cell classes that differ in self-renewal capacity. Nat Immunol 5: 738–743.
6. Dick JE (2008) Stem cell concepts renew cancer research. Blood 112: 4793–4807.
7. Becker MW, Jordan CT (2011) Leukemia stem cells in 2010: current understanding and future directions. Blood Rev 25: 75–81.
8. de The H, Chen Z (2010) Acute promyelocytic leukaemia: novel insights into the mechanisms of cure. Nat Rev Cancer 10: 775–783.
9. Paietta E (2003) Expression of cell-surface antigens in acute promyelocytic leukaemia. Best Pract Res Clin Haematol 16: 369–385.
10. Ito M, Hiramatsu H, Kobayashi K, Suzue K, Kawahata M, et al. (2002) NOD/SCID/gamma(c)(null) mouse: an excellent recipient mouse model for engraftment of human cells. Blood 100: 3175–3182.
11. Yahata T, Ando K, Nakamura Y, Ueyama Y, Shimamura K, et al. (2002) Functional human T lymphocyte development from cord blood CD34+ cells in nonobese diabetic/Shi-scid, IL-2 receptor gamma null mice. J Immunol 169: 204–209.
12. Patel S, Zhang Y, Cassinat B, Zassadowski F, Ferre N, et al. (2012) Successful xenografts of AML3 samples in immunodeficient NOD/shi-SCID IL2R-gamma(-/-) mice. Leukemia 26: 2432–2435.
13. Guibal FC, Alberich-Jorda M, Hirai H, Ebralidze A, Levantini E, et al. (2009) Identification of a myeloid committed progenitor as the cancer-initiating cell in acute promyelocytic leukemia. Blood 114: 5415–5425.
14. Wojiski S, Guibal FC, Kindler T, Lee BH, Jesneck JL, et al. (2009) PML-RARalpha initiates leukemia by conferring properties of self-renewal to committed promyelocytic progenitors. Leukemia 23: 1462–1471.
15. Brown D, Kogan S, Lagasse E, Weissman I, Alcalay M, et al. (1997) A PMLRARalpha transgene initiates murine acute promyelocytic leukemia. Proc Natl Acad Sci U S A 94: 2551–2556.
16. Grisolano JL, Wesselschmidt RL, Pelicci PG, Ley TJ (1997) Altered myeloid development and acute leukemia in transgenic mice expressing PML-RAR alpha under control of cathepsin G regulatory sequences. Blood 89: 376–387.
17. He LZ, Tribioli C, Rivi R, Peruzzi D, Pelicci PG, et al. (1997) Acute leukemia with promyelocytic features in PML/RARalpha transgenic mice. Proc Natl Acad Sci U S A 94: 5302–5307.
18. Westervelt P, Lane AA, Pollock JL, Oldfather K, Holt MS, et al. (2003) High-penetrance mouse model of acute promyelocytic leukemia with very low levels of PML-RARalpha expression. Blood 102: 1857–1865.
19. Grignani F, Valtieri M, Gabbianelli M, Gelmetti V, Botta R, et al. (2000) PML/RAR alpha fusion protein expression in normal human hematopoietic progenitors dictates myeloid commitment and the promyelocytic phenotype. Blood 96: 1531–1537.
20. Manz MG, Miyamoto T, Akashi K, Weissman IL (2002) Prospective isolation of human clonogenic common myeloid progenitors. Proc Natl Acad Sci U S A 99: 11872–11877.
21. Pear WS, Miller JP, Xu L, Pui JC, Soffer B, et al. (1998) Efficient and rapid induction of a chronic myelogenous leukemia-like myeloproliferative disease in mice receiving P210 bcr/abl-transduced bone marrow. Blood 92: 3780–3792.
22. Matsushita H, Scaglioni PP, Bhaumik M, Rego EM, Cai LF, et al. (2006) In vivo analysis of the role of aberrant histone deacetylase recruitment and RAR alpha blockade in the pathogenesis of acute promyelocytic leukemia. J Exp Med 203: 821–828.
23. Kawada H, Ando K, Tsuji T, Shimakura Y, Nakamura Y, et al. (1999) Rapid ex vivo expansion of human umbilical cord hematopoietic progenitors using a novel culture system. Exp Hematol 27: 904–915.
24. Yahata T, Takanashi T, Muguruma Y, Ibrahim AA, Matsuzawa H, et al. (2011) Accumulation of oxidative DNA damage restricts the self-renewal capacity of human hematopoietic stem cells. Blood 118: 2941–2950.

25. Rego EM, He LZ, Warrell RP Jr, Wang ZG, Pandolfi PP (2000) Retinoic acid (RA) and As2O3 treatment in transgenic models of acute promyelocytic leukemia (APL) unravel the distinct nature of the leukemogenic process induced by the PML-RARalpha and PLZF-RARalpha oncoproteins. Proc Natl Acad Sci U S A 97: 10173–10178.
26. Payton JE, Grieselhuber NR, Chang LW, Murakami M, Geiss GK, et al. (2009) High throughput digital quantification of mRNA abundance in primary human acute myeloid leukemia samples. J Clin Invest 119: 1714–1726.
27. Ando K, Yahata T, Sato T, Miyatake H, Matsuzawa H, et al. (2006) Direct evidence for ex vivo expansion of human hematopoietic stem cells. Blood 107: 3371–3377.
28. Schmidt M, Hoffmann G, Wissler M, Lemke N, Mussig A, et al. (2001) Detection and direct genomic sequencing of multiple rare unknown flanking DNA in highly complex samples. Hum Gene Ther 12: 743–749.
29. Dyck JA, Maul GG, Miller WH Jr, Chen JD, Kakizuka A, et al. (1994) A novel macromolecular structure is a target of the promyelocyte-retinoic acid receptor oncoprotein. Cell 76: 333–343.
30. Weis K, Rambaud S, Lavau C, Jansen J, Carvalho T, et al. (1994) Retinoic acid regulates aberrant nuclear localization of PML-RAR alpha in acute promyelocytic leukemia cells. Cell 76: 345–356.
31. Grignani F, Testa U, Rogaia D, Ferrucci PF, Samoggia P, et al. (1996) Effects on differentiation by the promyelocytic leukemia PML/RARalpha protein depend on the fusion of the PML protein dimerization and RARalpha DNA binding domains. EMBO J 15: 4949–4958.
32. Paietta E, Goloubeva O, Neuberg D, Bennett JM, Gallagher R, et al. (2004) A surrogate marker profile for PML/RAR alpha expressing acute promyelocytic leukemia and the association of immunophenotypic markers with morphologic and molecular subtypes. Cytometry B Clin Cytom 59: 1–9.
33. Welch JS, Ley TJ, Link DC, Miller CA, Larson DE, et al. (2012) The origin and evolution of mutations in acute myeloid leukemia. Cell 150: 264–278.
34. Welch JS, Yuan W, Ley TJ (2011) PML-RARA can increase hematopoietic self-renewal without causing a myeloproliferative disease in mice. J Clin Invest 121: 1636–1645.
35. Wartman LD, Welch JS, Uy GL, Klco JM, Lamprecht T, et al. (2012) Expression and function of PML-RARA in the hematopoietic progenitor cells of Ctsg-PML-RARA mice. PLoS One 7: e46529.
36. Puccetti E, Ruthardt M (2004) Acute promyelocytic leukemia: PML/RARalpha and the leukemic stem cell. Leukemia 18: 1169–1175.
37. Ferrucci PF, Grignani F, Pearson M, Fagioli M, Nicoletti I, et al. (1997) Cell death induction by the acute promyelocytic leukemia-specific PML/RARalpha fusion protein. Proc Natl Acad Sci U S A 94: 10901–10906.
38. Grignani F, Ferrucci PF, Testa U, Talamo G, Fagioli M, et al. (1993) The acute promyelocytic leukemia-specific PML-RAR alpha fusion protein inhibits differentiation and promotes survival of myeloid precursor cells. Cell 74: 423–431.
39. Collins SJ (2002) The role of retinoids and retinoic acid receptors in normal hematopoiesis. Leukemia 16: 1896–1905.
40. Du C, Redner RL, Cooke MP, Lavau C (1999) Overexpression of wild-type retinoic acid receptor alpha (RARalpha) recapitulates retinoic acid-sensitive transformation of primary myeloid progenitors by acute promyelocytic leukemia RARalpha-fusion genes. Blood 94: 793–802.
41. Thanopoulou E, Cashman J, Kakagianne T, Eaves A, Zoumbos N, et al. (2004) Engraftment of NOD/SCID-beta2 microglobulin null mice with multilineage neoplastic cells from patients with myelodysplastic syndrome. Blood 103: 4285–4293.
42. Kerbauy DM, Lesnikov V, Torok-Storb B, Bryant E, Deeg HJ (2004) Engraftment of distinct clonal MDS-derived hematopoietic precursors in NOD/SCID-beta2-microglobulin-deficient mice after intramedullary transplantation of hematopoietic and stromal cells. Blood 104: 2202–2203.
43. Muguruma Y, Matsushita H, Yahata T, Yumino S, Tanaka Y, et al. (2011) Establishment of a xenograft model of human myelodysplastic syndromes. Haematologica 96: 543–551.
44. Taussig DC, Vargaftig J, Miraki-Moud F, Griessinger E, Sharrock K, et al. (2010) Leukemia-initiating cells from some acute myeloid leukemia patients with mutated nucleophosmin reside in the CD34(-) fraction. Blood 115: 1976–1984.
45. Eppert K, Takenaka K, Lechman ER, Waldron L, Nilsson B, et al. (2011) Stem cell gene expression programs influence clinical outcome in human leukemia. Nat Med 17: 1086–1093.

PAI-1–regulated extracellular proteolysis governs senescence and survival in *Klotho* mice

Mesut Eren[a], Amanda E. Boe[a,b], Sheila B. Murphy[a,b], Aaron T. Place[a,b], Varun Nagpal[a,b], Luisa Morales-Nebreda[a], Daniela Urich[a], Susan E. Quaggin[a,b], G. R. Scott Budinger[a], Gökhan M. Mutlu[a], Toshio Miyata[c], and Douglas E. Vaughan[a,b,1]

[a]Department of Medicine and [b]Feinberg Cardiovascular Research Institute, Northwestern University Feinberg School of Medicine, Chicago, IL 60611; and [c]United Centers for Advanced Research and Translational Medicine, Tohoku University Graduate School of Medicine, Miyagi 980-8575, Japan

Edited* by David Ginsburg, University of Michigan Medical School, Ann Arbor, MI, and approved April 2, 2014 (received for review November 25, 2013)

Cellular senescence restricts the proliferative capacity of cells and is accompanied by the production of several proteins, collectively termed the "senescence-messaging secretome" (SMS). As senescent cells accumulate in tissue, local effects of the SMS have been hypothesized to disrupt tissue regenerative capacity. *Klotho* functions as an aging-suppressor gene, and *Klotho*-deficient (*kl/kl*) mice exhibit an accelerated aging-like phenotype that includes a truncated lifespan, arteriosclerosis, and emphysema. Because plasminogen activator inhibitor-1 (PAI-1), a serine protease inhibitor (SERPIN), is elevated in *kl/kl* mice and is a critical determinant of replicative senescence in vitro, we hypothesized that a reduction in extracellular proteolytic activity contributes to the accelerated aging-like phenotype of *kl/kl* mice. Here we show that PAI-1 deficiency retards the development of senescence and protects organ structure and function while prolonging the lifespan of *kl/kl* mice. These findings indicate that a SERPIN-regulated cell-nonautonomous proteolytic cascade is a critical determinant of senescence in vivo.

FGF23 | IGFBP3 | IL-6 | TM5441

Advanced age contributes to the development of frailty and disease in humans, but the fundamental mechanisms that drive physiological aging are incompletely understood (1, 2). Cellular senescence, which halts the proliferative capacity of cells, is associated with the manifestation of the senescence-associated secretory phenotype (3) and the production and secretion of a distinct set of proteins (2, 4), including insulin-like growth factor-binding proteins (IGFBPs), interleukins (ILs), transforming growth factor type β (TGF-β), and plasminogen activator inhibitor-1 (PAI-1) (5), collectively termed the "senescence-messaging secretome" (SMS) (6). In addition to this pattern of protein production and secretion, senescent cells display a distinctive morphology, and can be identified by increased expression of senescence-associated β-galactosidase (7). The tumor suppressor and proapoptotic protein p53 plays a central role in inducing replicative senescence by regulating the transcription of genes involved in cell cycle arrest and apoptosis, including the cyclin-dependent kinase inhibitors $p16^{Ink4a}$ and p21 (8). Senescence can be triggered by a number of factors, including DNA damage (9), oncogene induction (10), and oxidative stress (11). Although the relationship between cellular senescence and physiological aging remains an area of intense investigation, it is becoming increasingly evident that the two processes are fundamentally linked. Senescent cells accumulate in aging tissues and have been hypothesized to disrupt tissue regeneration, which may reflect cell-nonautonomous effects of the SMS (6).

In the last decade, numerous examples of genetically modified mice with phenotypes reminiscent of human aging have been described and investigated. These include the $BubR1^{H/H}$ progeroid (12) and *Klotho*-deficient (*kl/kl*) mice (13). $BubR1^{H/H}$ progeroid mice exhibit an age-dependent increase in the expression levels of PAI-1 in numerous locations, including white adipose tissue, skeletal muscle, and the eye (12). $BubR1^{H/H}$ mice have a shortened average lifespan (24 wk) and develop various aging-like phenotypic abnormalities, including sarcopenia, cataracts, arterial stiffening, and impaired wound healing (14). Klotho functions as an aging-suppressor protein by impeding the development of senescence in vitro and in vivo through inhibition of the Wnt (15), TGF-β (16), and IGF1 signaling pathways (17). Thus, *kl/kl* mice exhibit a rapidly progressive phenotype after weaning that includes a truncated lifespan (8–12 wk), renal sclerosis, arteriosclerosis, emphysema, and osteoporosis (13). Membrane-bound Klotho forms a heterodimer with fibroblast growth factor (FGF) receptors (FGFRs) generating a high-affinity receptor for FGF23. Signals transduced by FGF23 via the Klotho–FGFR complex inhibit 1,25-$(OH)_2$ vitamin D_3 and parathyroid hormone synthesis and promote renal phosphate excretion. *kl/kl* mice exhibit a remarkable increase in plasma levels of FGF23, as well as significant increases in serum levels of calcium, phosphate, vitamin D_3, and creatinine (13). Interestingly, *kl/kl* mice also have an age-dependent increase in plasma PAI-1 levels as well as increased PAI-1 expression in a number of tissues including kidney, aorta, and heart (18). Because PAI-1 is necessary and sufficient to induce replicative senescence in vitro downstream of p53 (19) and is markedly increased in *kl/kl* mice, we hypothesized that PAI-1 is a critical determinant of the phenotypic abnormalities developed by *kl/kl* mice. Here we examined the impact of PAI-1 on senescence and physiological aging in vivo by breeding *kl/kl* and PAI-1–deficient ($pai\text{-}1^{-/-}$) mice to generate *kl/kl* mice with partial ($kl/klpai\text{-}1^{+/-}$) or complete ($kl/klpai\text{-}1^{-/-}$) PAI-1 deficiency.

Results

PAI-1 Deficiency Prolongs the Survival of *kl/kl* Mice. We systematically monitored the effect of PAI-1 deficiency on the growth, vigor, and survival of littermate *kl/kl* ($n = 26$), $kl/klpai\text{-}1^{+/-}$ ($n = 39$), $kl/klpai\text{-}1^{-/-}$ ($n = 25$), and WT ($n = 16$) mice (Fig. 1) all in the

Significance

Plasminogen activator inhibitor-1 (PAI-1) is an essential mediator of cellular senescence in vitro and is one of the biochemical fingerprints of senescence in vivo. *Klotho*-deficient (*kl/kl*) mice display a complex phenotype reminiscent of human aging and exhibit age-dependent increases in PAI-1 in tissues and in plasma. Thus, we hypothesized that PAI-1 contributes to the aging-like phenotype of *kl/kl* mice. We observed that either genetic deficiency or pharmacological inhibition of PAI-1 in *kl/kl* mice was associated with reduced evidence of senescence, preserved organ structure and function, and a fourfold increase in median lifespan. These findings indicate that PAI-1 is a critical mediator of senescence in vivo and defines a novel target for the prevention and treatment of age-related disorders in man.

Author contributions: M.E. and D.E.V. designed research; M.E., A.E.B., S.B.M., A.T.P., V.N., L.M.-N., and D.U. performed research; T.M. contributed new reagents/analytic tools; M.E., S.E.Q., G.R.S.B., G.M.M., and D.E.V. analyzed data; and M.E. and D.E.V. wrote the paper.

The authors declare no conflict of interest.

*This Direct Submission article had a prearranged editor.

[1]To whom correspondence should be addressed. E-mail: d-vaughan@northwestern.edu.

This article contains supporting information online at www.pnas.org/lookup/suppl/doi:10.1073/pnas.1321942111/-/DCSupplemental.

same genetic background (75% C57BL/6J, 25% C3J). We observed that either partial or complete absence of PAI-1 prolonged the survival of *kl/kl* mice. Log-rank analysis indicated that the survival curves for the WT, *kl/kl*, *kl/klpai-1*$^{+/-}$, and *kl/klpai-1*$^{-/-}$ mice differed significantly ($P < 0.0001$). The median survival of *kl/kl* mice was 58 d, and this value increased with PAI-1 deficiency: 2.8-fold (163 d) in *kl/klpai-1*$^{+/-}$ mice and 4.2-fold (246 d) in *kl/klpai-1*$^{-/-}$ mice. Whereas all of the *kl/kl* mice died within 120 d, 65% of *kl/klpai-1*$^{+/-}$ and 82% of *kl/klpai-1*$^{-/-}$ mice were alive beyond 120 d. Although median survival indicates a dose–response relationship between genotype and mortality ($P = 0.0002$ by log-rank test for trend), the mean lifespan increased similarly in *kl/klpai-1*$^{+/-}$ (250 ± 169 d) and *kl/klpai-1*$^{-/-}$ (254 ± 123 d) mice (mean ± SD), corresponding to 4.2- and 4.5-fold increases, respectively. Furthermore, we achieved a similar prolongation of lifespan in *kl/kl* mice ($n = 11$) (Fig. 1*B*) by the administration of an orally active small-molecule PAI-1 antagonist, TM5441, whose pharmacokinetic properties, toxicity, and specificity have been described recently (20). In contrast with the inconsistent effects based on sex of a low phosphate diet on survival in *kl/kl* mice (21), both males and females appear to benefit from complete PAI-1 deficiency. However, survival of *kl/klpai-1*$^{+/-}$ females ($n = 19$) was not as long as that of males ($n = 20$) of the same genotype (median survival 121 d vs. 315 d, mean lifespan 208 ± 151 d vs. 285 ± 182, respectively; $P = 0.16$). Nevertheless, *kl/klpai-1*$^{+/-}$ females do live longer than *kl/kl* females ($n = 14$) (median survival 121 d vs. 58 d, mean lifespan 208 ± 151 d vs. 57 ± 18, respectively; $P = 0.0004$) (Fig. S1). This improvement in survival was also associated with evidence of increased overall vigor and health, as *kl/klpai-1*$^{-/-}$ mice exhibited near-normal weight gain over time (Fig. 1 *A* and *C*) and spontaneous physical activity (Fig. 1*D*).

PAI-1 Deficiency Normalizes Senescence and Telomere Length in *kl/kl* Mice. To characterize the extent of senescence in *kl/kl* mice and how PAI-1 deficiency affects it, plasma levels of the SMS factors IGFBP-3 and IL-6, and telomere length were measured in liver, aorta, tail, and kidney tissue. We observed that *kl/kl* mice had increased levels of IGFBP-3 (Fig. 2*A*) compared with WT mice ($P = 0.02$). With partial ($P = 0.03$ vs. *kl/kl* mice) or complete PAI-1 deficiency ($P = 0.02$ vs. *kl/kl* mice), IGFBP-3 levels did not significantly differ from those seen in WT mice. Similarly, we found that compared with levels in WT mice, *kl/kl* mice had a 13-fold increase ($P = 0.02$) in plasma levels of proinflammatory cytokine IL-6, which functions in the acquisition of the senescent phenotype in vitro (Fig. 2*B*). Compared with *kl/kl* mice, IL-6 levels were reduced by 79% in *kl/klpai-1*$^{+/-}$ ($P = 0.03$) and 83%

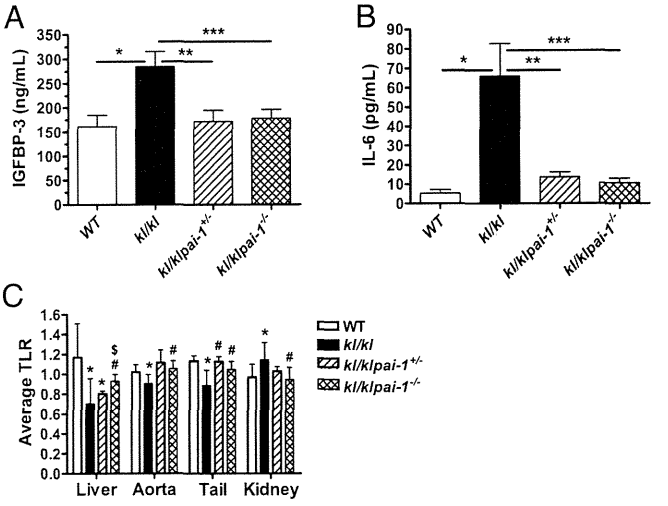

Fig. 2. Effect of PAI-1 deficiency on plasma levels of SMS factors and ATLR in various tissues from age-matched littermate *Klotho* mice. (*A*) Determination of IGFBP-3 levels in plasma samples ($n = 6$ per group). *$P = 0.02$, **$P = 0.03$, and ***$P = 0.02$. (*B*) Quantitation of circulating IL-6 levels ($n = 6$ to 14). *$P = 0.02$, **$P = 0.03$, and ***$P = 0.0001$. (*C*) Quantitation of ATLR by qRT-PCR in liver, aorta, tail, and kidney tissue ($n = 6$ to 14). *$P < 0.05$ compared with WT, #$P < 0.05$ compared with *kl/kl*, and $$P < 0.05$ compared with *kl/klpai-1*$^{+/-}$. Data are plotted as mean ± SD.

in *kl/klpai-1*$^{-/-}$ ($P = 0.0001$) mice. These observations suggest that the elevated PAI-1 levels in *kl/kl* mice are a dominant factor in contributing to increases in plasma IGFBP-3 and IL-6 and further augment the senescent phenotype in these mice.

Although elevated plasma levels of SMS components may reflect systemic senescence, they are nonspecific in nature and do not provide precise identification of which tissues are actually senescent. To address this limitation, telomere length was determined in several different tissues. Liver, aorta, and tail tissue samples from *kl/kl* mice displayed moderate but significant decreases in the average telomere length ratio (ATLR), whereas renal tissue had 16% longer ATLRs compared with those of WT animals (Fig. 2*C*). In contrast, ATLRs of liver and tail tissues from *kl/klpai-1*$^{+/-}$ and liver, aorta, and tail, tissues from *kl/klpai-1*$^{-/-}$ mice were significantly longer than those of *kl/kl* mice. These findings indicate that PAI-1 deficiency provides partial protection of telomere integrity in numerous tissues. The anomalous

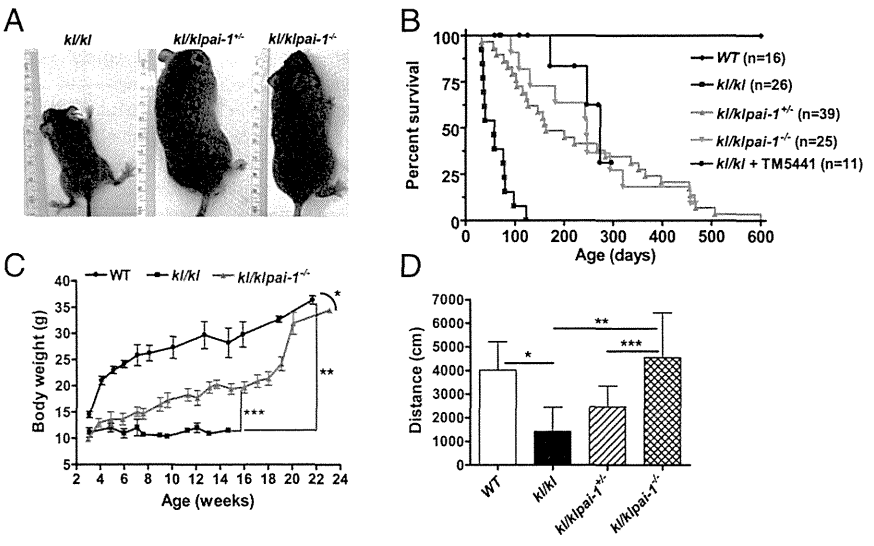

Fig. 1. Effects of PAI-1 deficiency in *Klotho* mice. (*A*) Size and appearance of 8-wk-old littermate mice. (*B*) Survival curve. Log-rank analysis showed that the survival curves for the WT, *kl/kl*, *kl/klpai-1*$^{+/-}$, and *kl/klpai-1*$^{-/-}$ mice differed significantly ($P < 0.0001$). (*C*) Bodyweight measurements starting from 3 wk of age. *$P = 0.002$, **$P = 0.0001$, and ***$P = 0.0003$. (*D*) Open field physical activity measurements recorded as distance traveled in 20 min in age-matched animals. *$P = 0.027$, **$P = 0.018$, and ***$P = 0.036$. Data are plotted as mean ± SD.

preservation of telomere length in renal tissue from *kl/kl* mice may reflect the lack of turnover in renal cells and the early induction of replicative senescence in the kidneys of *kl/kl* mice (22).

Because the kidneys are one of the most severely compromised organs in *kl/kl* mice, we also examined kidneys for biomarkers of senescence, including $p16^{Ink4a}$ and p21. We detected strong immunostaining for $p16^{Ink4a}$ localized in the nuclei of tubules in kidney tissues from *kl/kl* mice (Fig. 3), but not for p21. In contrast, kidney sections from *kl/klpai-1*$^{-/-}$ mice had only minimal evidence of $p16^{Ink4a}$ accumulation (Fig. 3). Quantitative real-time PCR (qRT-PCR) analysis showed that the relative expression of $p16^{Ink4a}$ in kidneys from *kl/kl* mice is 3.2-fold higher than that in WT mice ($P = 0.001$) (Fig. 3*E*). In *kl/klpai-1*$^{+/-}$ and *kl/klpai-1*$^{-/-}$ mice, $p16^{Ink4a}$ expression was reduced by 80% ($P = 0.04$) and 92% ($P = 0.0001$) compared with the *kl/kl* mice, respectively, and in *kl/klpai-1*$^{-/-}$ mice by 78% compared with the levels seen in WT animals ($P = 0.0001$).

Effect of PAI-1 Deficiency on the Biochemical Hallmarks of *kl/kl* Mice. In an effort to explain the effects of PAI-1 deficiency on the *kl/kl* phenotype, we measured plasma levels of factors that are biochemical hallmarks of *kl/kl* mice, including FGF23, vitamin D_3, calcium, phosphate, creatinine, and PAI-1 (Table 1). As expected, *kl/kl* mice displayed a more than 1,200-fold increase in FGF23 levels [$2.8 \times 10^5 \pm 1.4 \times 10^5$ pg/mL vs. 225 ± 65 pg/mL in WT mice ($P = 0.004$)], reflecting the loss of functioning receptors for FGF23. Both *kl/klpai-1*$^{+/-}$ and *kl/klpai-1*$^{-/-}$ mice exhibited a nearly 98% reduction in plasma FGF23 levels compared with *kl/kl* mice [$3.4 \times 10^3 \pm 2.1 \times 10^3$ pg/mL ($P < 0.0001$) and $3.9 \times 10^3 \pm 0.9 \times 10^3$ pg/mL ($P = 0.0001$), respectively]. Similarly, vitamin D_3 levels were reduced in *kl/klpai-1*$^{+/-}$ ($P = 0.032$) and *kl/klpai-1*$^{-/-}$ ($P = 0.0003$) mice compared with the levels in *kl/kl* mice. Interestingly, partial or complete PAI-1 deficiency had only a marginal impact on serum levels of calcium, phosphate, and creatinine in *kl/kl* mice. As expected, PAI-1 antigen was not detectable in plasma from *kl/klpai-1*$^{-/-}$ mice, and levels in *kl/klpai-1*$^{+/-}$ animals were reduced by nearly 50% compared with those from *kl/kl* mice ($P < 0.05$). In addition, PAI-1 expression levels were reduced in tissues from *kl/klpai-1*$^{+/-}$ mice compared with those of *kl/kl* mice (Fig. S2).

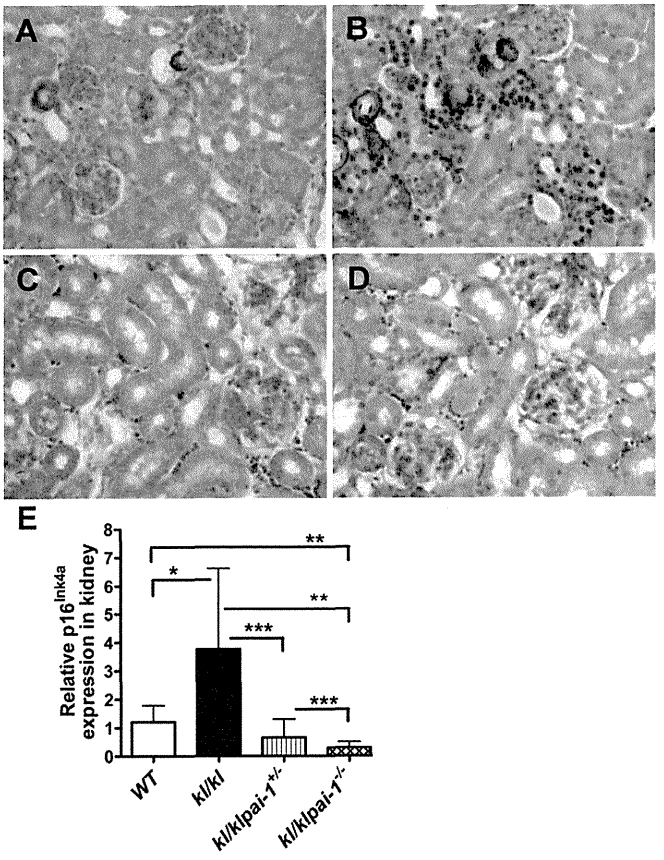

Fig. 3. Effect of PAI-1 deficiency on renal $p16^{Ink4a}$ expression in *Klotho*-deficient mice. (*A* and *C*) Control immunostaining of kidney sections from *kl/kl* and *kl/klpai-1*$^{-/-}$ mice, respectively, in the absence of the anti-$p16^{Ink4a}$ antibody. (*B* and *D*) Immunodetection of $p16^{Ink4a}$-positive cells in kidney sections from *kl/kl* and *kl/klpai-1*$^{-/-}$ mice, respectively. (*E*) Quantitation of relative $p16^{Ink4a}$ expression in the kidney. qRT-PCR analysis was performed on total RNA samples purified from WT ($n = 8$), *kl/kl* ($n = 6$), *kl/klpai-1*$^{+/-}$ ($n = 4$), and *kl/klpai-1*$^{-/-}$ ($n = 8$) kidneys. *$P = 0.001$, **$P = 0.0001$, and ***$P = 0.04$. Data are plotted as mean ± SD. (Magnification: *A–D*, 60×.)

PAI-1 Deficiency Preserves Organ Structure in *kl/kl* Mice. As reported previously, *kl/kl* mice develop emphysema that is characterized by a progressive, age-dependent enlargement of air spaces and associated alveolar destruction (Fig. 4) (23). Histological analysis of lung tissues from *kl/klpai-1*$^{+/-}$ and *kl/klpai-1*$^{-/-}$ (Fig. 4) mice showed that PAI-1 deficiency primarily prevents alveolar enlargement. Consistent with the preservation of pulmonary structural integrity, pulmonary function was also maintained with PAI-1 deficiency. We found that *kl/kl* mice had a 40% decrease in PaO_2 levels ($P = 0.018$) in arterial blood samples. Arterial oxygenation normalized with partial ($P = 0.05$) and complete ($P = 0.02$) PAI-1 deficiency in *kl/kl* mice (Fig. 4*E*). These results indicate that PAI-1 is an important contributor to the emphysematous changes observed in *kl/kl* mice.

Finally, we analyzed mice for evidence of ectopic calcification, which has been reported to increase with age in *kl/kl* mice. Whereas the age-matched WT littermate mice had no detectable calcification, we observed prominent calcium deposits in the kidneys of *kl/kl* mice (Fig. 5 *A* and *B*) ($P = 0.002$). However, analysis of kidneys from *kl/klpai-1*$^{+/-}$ (Fig. 5*C*) and *kl/klpai-1*$^{-/-}$ (Fig. 5*D*) mice showed that ectopic calcification areas were significantly reduced by 41% ($P = 0.03$) and 96% ($P < 0.0001$), respectively. To test the effect of PAI-1 deficiency on the impaired osteogenic signaling observed in *kl/kl* mice (24, 25), we measured the serum levels of aldosterone and alkaline phosphatase (ALP) activity (Table 1). Although aldosterone levels were significantly higher in *kl/kl* mice than that of WT animals, it was not altered significantly in *kl/klpai-1*$^{-/-}$ mice. Furthermore, we did not observe any difference in ALP activity among the mice groups studied here. This observation indicates that partial or complete loss of PAI-1 expression protects against age-induced ectopic calcification in *kl/kl* mice without altering serum levels of phosphate, calcium, ALP and aldosterone.

Discussion

PAI-1 is expressed in senescent cells and tissues, and is recognized as a primary component of the SMS. Most mammalian models of aging investigated thus far exhibit evidence of increased PAI-1 expression (12, 14). Furthermore, genetic or therapeutic interventions that prolong survival or reduce senescence in tissues in vivo are coincidentally associated with reductions in PAI-1. To our knowledge, this in vivo study is the first to investigate systematically the role of PAI-1 not only in the development of senescence, but also in the aging-like pathology of a mammal. The results from this study suggest that the onset of physiological aging can be delayed by modulating PAI-1, which subsequently prevents the nuclear accumulation of senescence marker $p16^{Ink4a}$ and maintains the structural and functional integrity of vital organs. Furthermore, the ability of a small-molecule PAI-1 antagonist to augment survival to a similar extent in *kl/kl* mice indicates that the observed effects are likely cell-nonautonomous. The protective effects of partial or complete PAI-1 deficiency are in agreement with previous work from our laboratory indicating that transgenic overexpression of

Table 1. Effects of PAI-1 deficiency on blood levels of the biochemical hallmarks of *klotho* mice

Circulating factors assayed	WT $n = 4$ to 5	*kl/kl* $n = 6$ to 9	*kl/klpai-1*$^{+/-}$ $n = 5$ to 6	*kl/klpai-1*$^{-/-}$ $n = 6$ to 10
Phosphate, mg/dL	7.7 ± 1.6	14.0 ± 2.8*	10.8 ± 2.6*	12.6 ± 2.7*
Calcium, mg/dL	7.9 ± 0.6	10.4 ± 0.9*	10.1 ± 1.2*	10.6 ± 0.8*
Creatinine, mg/dL	0.22 ± 0.11	0.31 ± 0.33	0.21 ± 0.11	0.18 ± 0.06
PAI-1, ng/mL	1.8 ± 0.4	45.2 ± 4.8*	24.3 ± 2.7*	0.0
FGF23, pg/mL	225 ± 65	295,657 ± 139,709*	3,924 ± 1,316*,#	3,795 ± 870*,#
Vitamin D_3, pg/mL	ND	1359 ± 145	698 ± 419#	314 ± 244#
Aldosterone, pg/mL	102 ± 20	160 ± 55*	ND	223 ± 96*
ALP, U/mL	20 ± 7	21 ± 6	17 ± 7	19 ± 5

ND, not determined.
*$P < 0.05$ compared with WT.
#$P < 0.05$ compared with *kl/kl*.

PAI-1 is sufficient to induce several aging-like phenotypic abnormalities, including age-dependent spontaneous coronary thrombosis, systemic amyloid deposition, and hair loss (26).

The normalization of FGF23 and vitamin D_3 levels in partial or complete PAI-1 knockout models strongly indicates that PAI-1 directly influences FGF23 signaling in *kl/kl* mice. Recent observations demonstrate that FGF23 is highly sensitive to cleavage by the serine protease furin, which is rapidly inhibited by PAI-1 (27, 28). In addition to FGF23, *kl/kl* mice have augmented expression of other furin substrates, including IGF1, TGF-β, MMP2, and MMP9 (29, 30). PAI-1 is known to regulate the proteolytic activation and/or clearance of many of these proteins. The precise identity and function of other proteases that are inhibited by PAI-1 and that contribute to the *Klotho* phenotype merits further investigation.

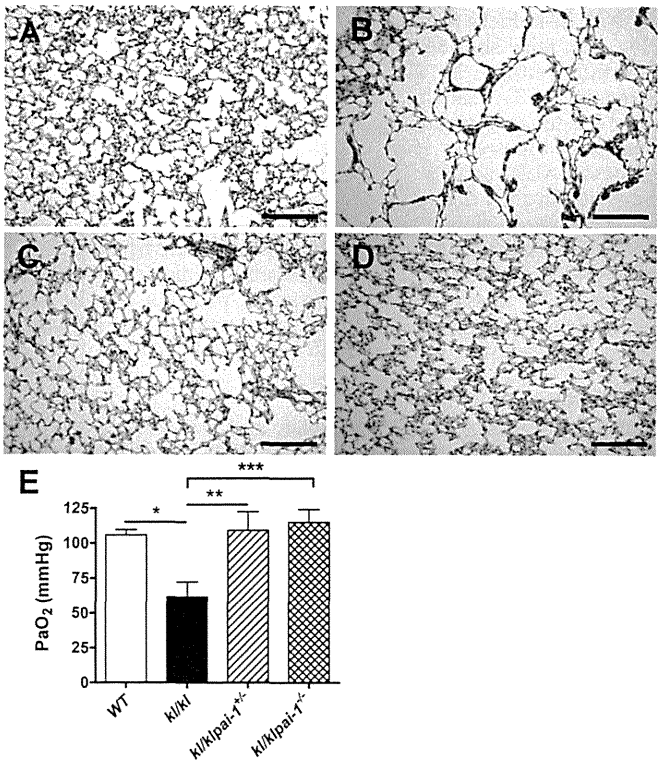

Fig. 4. Effects of PAI-1 deficiency on lung morphology and function. Masson's trichrome staining of lung sections in (*A*) WT, (*B*) *kl/kl*, (*C*) *kl/klpai-1*$^{+/-}$, and (*D*) *kl/klpai-1*$^{-/-}$ mice. (Scale bars: 150 μm.) (*E*) Partial pressure of oxygen (PaO_2) measurements in arterial blood ($n = 4$ for each group). *$P = 0.018$, **$P = 0.05$, and ***$P = 0.02$. Data are plotted as mean ± SD.

Because FGF23 signaling is impaired in *kl/kl* mice, the negative feedback inhibition on vitamin D_3 synthesis is dysfunctional. High vitamin D_3 and phosphate levels in *kl/kl* mice likely stimulate FGF23 synthesis in bone continuously, whereas the elevated PAI-1 levels reduce the proteolytic clearance of FGF23. Together, these combined effects on production, signaling, and metabolism likely explain the >1,200-fold increase in plasma FGF23 levels observed in *kl/kl* mice. Recent reports indicate that dietary deficiency of phosphate, zinc, and calcium significantly improves the lifespan of klotho mice (21, 25, 31). Although we did not detect any significant changes in the levels of phosphate and calcium in *kl/klpai-1*$^{-/-}$ mice, we observed that PAI-1 deficiency significantly prolongs the survival of *kl/kl* mice indicating that, in addition to the mineral homeostasis, PAI-1–regulated extracellular proteolysis strongly influences the aging phenotype.

Our findings also reveal a previously unrecognized role of PAI-1 in modulating the effects of FGF23. The increased plasma levels of PAI-1 in *kl/kl* mice are not surprising, but deserve some mechanistic explanation. Numerous factors likely contribute to the *Klotho* phenotype, and prominent on that list are the effects of TGF-β (16), Wnt (15), and IGF1 (17, 32). Importantly, all three of these factors can directly induce PAI-1 expression. As the phenotype matures, PAI-1 production is likely further augmented by the effects of progressive hypoxemia, the induction of the p53 pathway, aldosterone excess (25), and elevated levels of other components of the SMS, including IL-6, interferons, TGF-β, and IGFBPs.

Discovery of the *Klotho* gene has shed light into the molecular mechanisms of tissue calcification. The elevated phosphate and calcium levels in *kl/kl* mice certainly contribute to the pattern of ectopic calcification (33, 34). Recently, hyperaldosteronism was reported to be the major inducer of the osteog enic signaling, which was partially reversed by spironolactone without normalizing plasma levels of vitamin D_3, FGF23, calcium, and phosphate (24, 25). Furthermore, Lim et al. reported that FGF23 treatment reduced the aldosterone-induced expression of osteogenic factors in vitro (35). In addition, PAI-1 deficiency drastically reduced FGF23 levels and calcification without altering aldosterone and ALP levels in *kl/kl* mice (Table 1). These findings suggest that PAI-1, which is regulated by aldosterone (36), plays an unexpected but pivotal role in tissue calcification. The reduced plasma levels of vitamin D_3 and prevention of tissue calcification in *kl/klpai-1*$^{-/-}$ mice require the restoration of Klotho-independent FGF23 signaling. The present study strongly indicates that PAI-1 plays a direct role in the regulation of FGF23 signaling in *kl/kl* mice.

The reduced IGFBP-3 levels in *kl/kl* mice provide an important mechanistic insight into the protective effects of PAI-1 deficiency on the *Klotho* phenotype. It was recently demonstrated that the PAI-1–IGFBP-3 cascade promotes stress-induced senescence in human breast fibroblasts (37). Expression levels of IGFBP-3 are increased in response to senescence-inducing stimuli. However, the proteolytic metabolism of IGFBP-3 by tissue-type plasminogen activator (t-PA) prevents the induction of cellular

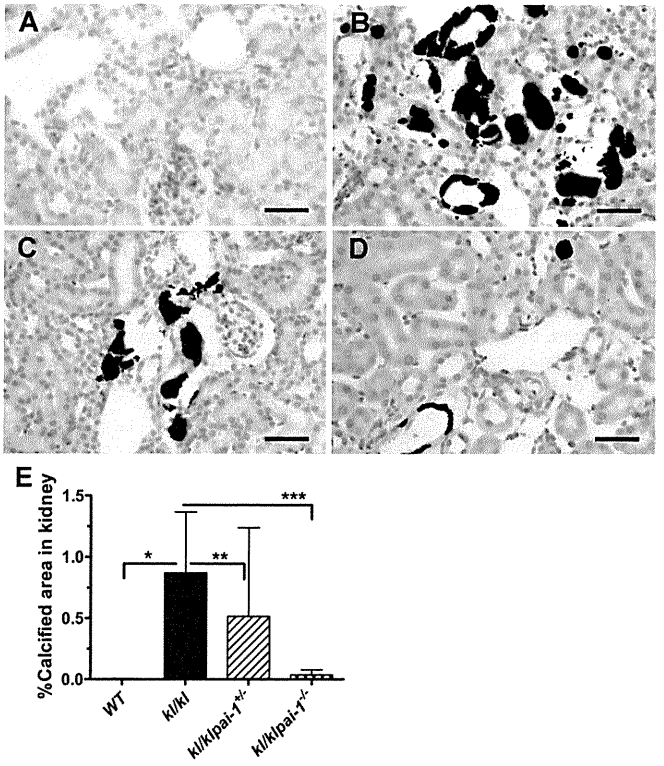

Fig. 5. Effects of PAI-1 deficiency on ectopic calcification characterized by von Kossa staining. Ectopic calcification analysis was performed on kidney ($n = 5$ for each group) sections. Although samples from (*A*) WT mice showed no detectable calcification, kidney sections from (*B*) *kl/kl* mice had remarkable calcified deposits. (*C*) Partial (*kl/klpai-1*$^{+/-}$) or (*D*) complete PAI-1 deficiency (*kl/klpai-1*$^{-/-}$), on the other hand, significantly decreased calcification levels. (Scale bars: 40 μm.) (*E*) Quantitative analyses using Image-Pro-6.3 software showed that the percentages of calcified areas in kidneys were reduced by 41% in *kl/klpai-1*$^{+/-}$ and 96% in *kl/klpai-1*$^{-/-}$ mice compared with *kl/kl* mice. $*P = 0.002$, $**P = 0.03$, and $***P = 0.0001$. Data are plotted as mean ± SD.

senescence in vitro. Because PAI-1 is the main physiological inhibitor of t-PA, IGFBP-3 appears to be a critical downstream target of PAI-1–induced senescence. These findings provide a possible mechanistic explanation for the prosenescent effects of increased PAI-1 in *kl/kl* mice and suggest a role for an extracellular cascade of secreted proteins in the regulation of cellular senescence and physiological aging.

It was recently shown that membrane-bound Klotho prevents the retinoic-acid-inducible gene-I–induced expression of IL-6 and -8 both in vitro and in vivo, suggesting that the antiaging function of Klotho also includes the suppression of inflammation (38). It is interesting to note that with PAI-1 deficiency, levels of both IGFBP-3 and IL-6 were normalized in *kl/kl* mice. This confirms and extends the recent observations by López-Andrés et al. that modulating the activity of a key member of the SMS can also normalize the levels of other SMS factors (39). This indicates that IGFBP-3 and IL-6 are downstream from PAI-1 in the senescence pathway.

In human fibroblasts, telomere shortening initiates senescence through a pathway that involves ataxia telangiectasia mutated (ATM), p53, and p21^{CIP1}, but not p16^{Ink4a} (9). Thus, the presence of p16^{Ink4a}-positive but not p21-positive cells in kidneys of *kl/kl* mice suggests that the pathway to senescence and accelerated aging in the renal tissue of *kl/kl* mice is likely mediated by p16^{Ink4a} and occurs independently of the p53 pathway. These findings in the kidney of preserved telomere length, together with augmented p16^{Ink4a} expression, suggest that renal cells undergo senescence without the requisite cellular division to shorten telomeres (22).

The results presented here indicate that PAI-1 is a critical contributor to, and not merely a marker of, senescence in vivo (12), and that novel therapies targeting PAI-1 or other components of the SMS (40) may prevent senescence and age-related pathologic changes in humans, including arteriosclerosis and emphysema. The development of small-molecule, orally active, selective PAI-1 antagonists, such as TM5441 and others (41), will allow these hypotheses to be tested prospectively.

Materials and Methods

Animals and Animal Care. The original genetic background of *kl/kl* mice, a kind gift from Makoto Kuro-o (Jichi Medial University, Shimotsuke, Tochigi, Japan), was composed of C57BL/6J and C3H/J (13). PAI-1–deficient mice were obtained from The Jackson Laboratory (background strain C57BL/6J; strain name B6.129S2-Serpine1tm1Mlg/J; stock no. 002507). *Klotho* mice and PAI-1–deficient mice were crossed to generate the heterozygous dihybrid mice (*KL/kl-pai-1*$^{+/-}$). All mice used in this study were littermates generated by breeding these *KL/kl-pai-1*$^{+/-}$ mice and thus of the same mixed background. They were housed in a temperature-controlled environment with a daily 14:10 h light–dark cycle and had unlimited access to food (standard rodent chow diet; Harlan Teklad) and water. All experimental protocols were approved by the Institutional Animal Care and Use Committee of Northwestern University.

PAI-1 Inhibitor TM5441. TM5441 was derived from the original hit compound TM5007 (42) and the lead compound TM5275 (43) through an extensive structure-activity relationship (44). We have recently described the pharmacokinetic properties and toxicity, and specificity of TM5441 (20). TM5441 was administered at 100 mg/kg·d^{-1} mixed in the chow.

Histological Methods. Tissues harvested from mice were fixed in formalin for 24–48 h and then processed overnight and embedded in paraffin. Tissues sectioned at 6-μm thickness were stained with Masson's trichrome to visualize tissue morphology. Ectopic calcification was analyzed by von Kossa staining of kidneys ($n = 5$ for each study group). The extent of calcification was quantified in multiple kidney sections from each mouse by using Image-Pro-6.3 image-processing software and the results presented as the percent calcified areas in kidneys (Fig. 3). To detect the senescent cells, tissue sections were immunostained overnight at 4 °C with a primary antibody to p16^{Ink4a} antigen (Cell Applications), and then the antigen was visualized with an HRP-conjugated secondary antibody (goat anti-mouse IgG at 1:500 dilution; Santa Cruz Biotechnology, Inc.). One-Step AEC Solution (BioGenex) was used as the substrate for antigen detection.

Quantitation of Factors in Plasma and Serum. Plasma levels of IGFBP-3, IL-6, and FGF23 were measured using the ELISA kits Quantikine Immunoassay kit from R&D Systems (catalog no. MGB300), Becton-Dickinson (catalog no. 555220), and Immutopics (catalog no. 60-6300), respectively, by following the manufacturers' suggested protocols. Vitamin D_3 levels in plasma were measured using the mouse 1,25-$(OH)_2$VitD3 HVD3 ELISA kit from NovaTein Biosciences (catalog no. NB-E20523). Calcium (catalog no. 0150-250), creatinine (catalog no. 0430-120), and phosphate (catalog no. 0830-125) levels were determined by using kits from Stanbio Laboratories. Plasma PAI-1 levels were measured with the Murine PAI-1 Total Antigen Assay from Molecular Innovations. A colorimetric assay kit and an ELISA kit from Abcam were used to measure serum levels of ALP and aldosterone (catalog nos. ab83369 and ab136933, respectively).

Measuring Partial Oxygen Pressure in Arterial Blood. PaO_2 levels in the arterial blood were measured in mice anesthetized with pentobarbital (75 mg/kg body weight, administered i.p.). After adequate anesthesia was achieved, we performed a tracheostomy and sutured a 20-gauge angiocatheter into the trachea. Mice were then placed on a small rodent ventilator (MiniVent; Harvard Apparatus) with the following settings: a respiratory rate of 150 breaths per minute, a tidal volume of 8 mL/kg body weight, and an FiO_2 of 0.21 (room air) as described previously (45). The animals were ventilated for 15 min before a thoracotomy was performed and then 200 μL arterial blood were collected into a heparinized syringe via direct puncture of the left ventricle. The arterial blood sample was processed for gas analysis using the Stat Profile pHOx blood gas analyzer (Nova Biomedical).

Quantitation of ATLR. Genomic DNA isolated from various tissues was used to measure telomere length by qRT-PCR as previously described with minor modification (46, 47). Briefly, telomere repeats were amplified using specially designed primers, which were then compared with the amplification of

a single-copy gene, the 36B4 gene (acidic ribosomal phosphoprotein PO), to determine the ATLR. One hundred nanograms of genomic DNA template were added to each 20 μL reaction containing forward and reverse primers (250 nM each for telomere primers, and 500 nM each for the 36B4 primers), SsoAdvanced SYBR Green Supermix (Bio-Rad USA), and nuclease-free water. A serially diluted standard curve of 100 ng to 3.125 ng per well of template DNA from a WT mouse sample was included on each plate for both the telomere and the 36B4 reactions to facilitate ATLR calculation. Critical values were converted to nanogram values according to the standard curves, and nanogram values of the telomere (T) reaction were divided by the nanogram values of the 36B4 (S) reaction to yield the ATLR. The primer sequences for the telomere portion were as follows: 5′-CGG TTT GTT TGG GTT TGG GTT TGG GTT TGG GTT TGG GTT-3′ and 5′-GGC TTG CCT TAC CCT TAC CCT TAC CCT TAC CCT TAC CCT-3′. The primer sequences for the 36B4 single copy gene portion were as follows: 5′-ACT GGT CTA GGA CCC GAG AAG-3′ and 5′-TCA ATG GTG CCT CTG GAG ATT-3′. Cycling conditions for both primer sets (run in the same plate) were 95 °C for 10 min, 30 cycles of 95 °C for 15 s, and 55 °C for 1 min for annealing and extension.

qRT-PCR. Tissues harvested from subject mice were snap-frozen in liquid nitrogen. Excess tissue was removed under a dissecting microscope. RNA was isolated using the Qiagen RNAeasy Mini Kit (Qiagen) using the manufacturer's protocol. cDNA was generated from the RNA using the qScript cDNA Supermix (Quanta Biosciences). qRT-PCR was performed using the SsoAdvanced SYBR Green Supermix (Bio-Rad USA). Forward and reverse primers used for $p16^{Ink4a}$ expression were, respectively: 5′-AGGGCCGTGTGCATGACGTG-3′ and 5′-GCACCGGGCGGGAGAAGGTA-3′; for PAI-1 expression, respectively: 5′-ACGCCTGGTGCTGGTGAATGC-3′ and 5′-ACGGTGCTGCCATCAGACTTGTG-3′; and for GAPDH expression, respectively: 5′-ATGTTCCAGTATGACTCCACTCACG-3′ and 5′-GAAGACACCAGTAGACTCCACGACA-3′ (IDT, Inc.).

Behavioral Characterization. To test the effect of PAI-1 deficiency on the level of physical activity of *kl/kl* mice, the open field test for spontaneous horizontal activity was performed on age-matched animals at the Northwestern University Mouse Behavioral Phenotyping Core Laboratory as described previously (13).

Statistical Analyses. We present the averaged values obtained for each study as mean ± SD. Statistical significance was assigned to a comparison by using an unpaired, two-tailed Student *t* test when comparing two groups. Statistical significance for the survival of groups was established by the log-rank analysis of Kaplan–Meier plots using GraphPad Prism 4 software. $P < 0.05$ was considered statistically significant.

ACKNOWLEDGMENTS. We thank Dr. Makoto Kuro-o for providing us with the *kl/kl* mice. We also thank Marissa Michaels for her help in obtaining reagents and coordinating various aspects of our projects. This work was supported by National Institutes of Health (NIH)/National Heart, Lung, and Blood Institute Grants 2R01HL051387 and 1P01HL108795. A.T.P. is supported in part by NIH National Institute of Diabetes and Digestive and Kidney Diseases Training Grant T32 KD007169.

1. Rodier F, Campisi J (2011) Four faces of cellular senescence. *J Cell Biol* 192(4):547–556.
2. Campisi J, d'Adda di Fagagna F (2007) Cellular senescence: When bad things happen to good cells. *Nat Rev Mol Cell Biol* 8(9):729–740.
3. Coppé JP, Desprez PY, Krtolica A, Campisi J (2010) The senescence-associated secretory phenotype: The dark side of tumor suppression. *Annu Rev Pathol* 5:99–118.
4. Krtolica A, Parrinello S, Lockett S, Desprez PY, Campisi J (2001) Senescent fibroblasts promote epithelial cell growth and tumorigenesis: A link between cancer and aging. *Proc Natl Acad Sci USA* 98(21):12072–12077.
5. Mu XC, Higgins PJ (1995) Differential growth state-dependent regulation of plasminogen activator inhibitor type-1 expression in senescent IMR-90 human diploid fibroblasts. *J Cell Physiol* 165(3):647–657.
6. Kuilman T, Peeper DS (2009) Senescence-messaging secretome: SMS-ing cellular stress. *Nat Rev Cancer* 9(2):81–94.
7. Dimri GP, et al. (1995) A biomarker that identifies senescent human cells in culture and in aging skin in vivo. *Proc Natl Acad Sci USA* 92(20):9363–9367.
8. Wahl GM, Carr AM (2001) The evolution of diverse biological responses to DNA damage: Insights from yeast and p53. *Nat Cell Biol* 3(12):E277–E286.
9. Herbig U, Jobling WA, Chen BP, Chen DJ, Sedivy JM (2004) Telomere shortening triggers senescence of human cells through a pathway involving ATM, p53, and p21 (CIP1), but not p16(INK4a). *Mol Cell* 14(4):501–513.
10. Serrano M, Lin AW, McCurrach ME, Beach D, Lowe SW (1997) Oncogenic ras provokes premature cell senescence associated with accumulation of p53 and p16INK4a. *Cell* 88(5):593–602.
11. Parrinello S, et al. (2003) Oxygen sensitivity severely limits the replicative lifespan of murine fibroblasts. *Nat Cell Biol* 5(8):741–747.
12. Baker DJ, et al. (2011) Clearance of p16Ink4a-positive senescent cells delays ageing-associated disorders. *Nature* 479(7372):232–236.
13. Kuro-o M, et al. (1997) Mutation of the mouse klotho gene leads to a syndrome resembling ageing. *Nature* 390(6655):45–51.
14. Baker DJ, et al. (2008) Opposing roles for p16Ink4a and p19Arf in senescence and ageing caused by BubR1 insufficiency. *Nat Cell Biol* 10(7):825–836.
15. Liu H, et al. (2007) Augmented Wnt signaling in a mammalian model of accelerated aging. *Science* 317(5839):803–806.
16. Doi S, et al. (2011) Klotho inhibits transforming growth factor-beta1 (TGF-beta1) signaling and suppresses renal fibrosis and cancer metastasis in mice. *J Biol Chem* 286(10):8655–8665.
17. Kurosu H, et al. (2005) Suppression of aging in mice by the hormone Klotho. *Science* 309(5742):1829–1833.
18. Takeshita K, et al. (2002) Increased expression of plasminogen activator inhibitor-1 with fibrin deposition in a murine model of aging, "Klotho" mouse. *Semin Thromb Hemost* 28(6):545–554.
19. Kortlever RM, Higgins PJ, Bernards R (2006) Plasminogen activator inhibitor-1 is a critical downstream target of p53 in the induction of replicative senescence. *Nat Cell Biol* 8(8):877–884.
20. Boe AE, et al. (2013) Plasminogen activator inhibitor-1 antagonist TM5441 attenuates Nω-nitro-L-arginine methyl ester-induced hypertension and vascular senescence. *Circulation* 128(21):2318–2324.
21. Morishita K, et al. (2001) The progression of aging in klotho mutant mice can be modified by dietary phosphorus and zinc. *J Nutr* 131(12):3182–3188.
22. Coviello-McLaughlin GM, Prowse KR (1997) Telomere length regulation during postnatal development and ageing in Mus spretus. *Nucleic Acids Res* 25(15):3051–3058.
23. Suga T, et al. (2000) Disruption of the klotho gene causes pulmonary emphysema in mice. Defect in maintenance of pulmonary integrity during postnatal life. *Am J Respir Cell Mol Biol* 22(1):26–33.
24. Voelkl J, et al. (2013) Spironolactone ameliorates PIT1-dependent vascular osteoinduction in klotho-hypomorphic mice. *J Clin Invest* 123(2):812–822.
25. Fischer SS, et al. (2010) Hyperaldosteronism in Klotho-deficient mice. *Am J Physiol Renal Physiol* 299(5):F1171–F1177.
26. Eren M, Painter CA, Atkinson JB, Declerck PJ, Vaughan DE (2002) Age-dependent spontaneous coronary arterial thrombosis in transgenic mice that express a stable form of human plasminogen activator inhibitor-1. *Circulation* 106(4):491–496.
27. Bernot D, et al. (2011) Plasminogen activator inhibitor 1 is an intracellular inhibitor of furin proprotein convertase. *J Cell Sci* 124(Pt 8):1224–1230.
28. Fukumoto S (2005) Post-translational modification of Fibroblast Growth Factor 23. *Ther Apher Dial* 9(4):319–322.
29. Thomas G (2002) Furin at the cutting edge: From protein traffic to embryogenesis and disease. *Nat Rev Mol Cell Biol* 3(10):753–766.
30. Tian S, Huang Q, Fang Y, Wu J (2011) FurinDB: A Database of 20-Residue Furin Cleavage Site Motifs, Substrates and Their Associated Drugs. *Int J Mol Sci* 12(2):1060–1065.
31. Razzaque MS (2009) The FGF23-Klotho axis: Endocrine regulation of phosphate homeostasis. *Nat Rev Endocrinol* 5(11):611–619.
32. Yamamoto M, et al. (2005) Regulation of oxidative stress by the anti-aging hormone klotho. *J Biol Chem* 280(45):38029–38034.
33. Hu MC, et al. (2011) Klotho deficiency causes vascular calcification in chronic kidney disease. *J Am Soc Nephrol* 22(1):124–136.
34. Ohnishi M, Nakatani T, Lanske B, Razzaque MS (2009) Reversal of mineral ion homeostasis and soft-tissue calcification of klotho knockout mice by deletion of vitamin D 1alpha-hydroxylase. *Kidney Int* 75(11):1166–1172.
35. Lim K, et al. (2012) Vascular Klotho deficiency potentiates the development of human artery calcification and mediates resistance to fibroblast growth factor 23. *Circulation* 125(18):2243–2255.
36. Brown NJ, et al. (2000) Aldosterone modulates plasminogen activator inhibitor-1 and glomerulosclerosis in vivo. *Kidney Int* 58(3):1219–1227.
37. Elzi DJ, et al. (2012) Plasminogen activator inhibitor 1—insulin-like growth factor binding protein 3 cascade regulates stress-induced senescence. *Proc Natl Acad Sci USA* 109(30):12052–12057.
38. Liu F, Wu S, Ren H, Gu J (2011) Klotho suppresses RIG-I-mediated senescence-associated inflammation. *Nat Cell Biol* 13(3):254–262.
39. López-Andrés N, et al. (2013) Absence of cardiotrophin 1 is associated with decreased age-dependent arterial stiffness and increased longevity in mice. *Hypertension* 61(1):120–129.
40. Peeper DS (2011) Ageing: Old cells under attack. *Nature* 479(7372):186–187.
41. Tashiro Y, et al. (2012) Inhibition of PAI-1 induces neutrophil-driven neoangiogenesis and promotes tissue regeneration via production of angiocrine factors in mice. *Blood* 119(26):6382–6393.
42. Izuhara Y, et al. (2008) Inhibition of plasminogen activator inhibitor-1: Its mechanism and effectiveness on coagulation and fibrosis. *Arterioscler Thromb Vasc Biol* 28(4):672–677.
43. Izuhara Y, et al. (2010) A novel inhibitor of plasminogen activator inhibitor-1 provides antithrombotic benefits devoid of bleeding effect in nonhuman primates. *J Cereb Blood Flow Metab* 30(5):904–912.
44. Miyata T, Yamaoka N, Kodama H, Murano K (2011) Inhibitor of plasminogen activator inhibitor-1. US Patent Appl 2,011,112,140 A1 (May 12, 2011).
45. Mutlu GM, et al. (2004) Upregulation of alveolar epithelial active Na+ transport is dependent on beta2-adrenergic receptor signaling. *Circ Res* 94(8):1091–1100.
46. Cawthon RM (2002) Telomere measurement by quantitative PCR. *Nucleic Acids Res* 30(10):e47.
47. Callicott RJ, Womack JE (2006) Real-time PCR assay for measurement of mouse telomeres. *Comp Med* 56(1):17–22.

STEM CELLS®

TISSUE-SPECIFIC STEM CELLS

Inhibition of Plasminogen Activator Inhibitor Type-1 Activity Enhances Rapid and Sustainable Hematopoietic Regeneration

ABD AZIZ IBRAHIM,[a,b] TAKASHI YAHATA,[a,c] MAKOTO ONIZUKA,[a,b] TAKASHI DAN,[d] CHARLES VAN YPERSELE DE STRIHOU,[e] TOSHIO MIYATA,[d] KIYOSHI ANDO[a,b]

Key Words. Hematopoietic stem cells • Bone marrow stromal cells • Hematopoiesis • Stem cell transplantation • Tissue regeneration • Osteoblast

[a]Division of Hematopoiesis, Research Center for Regenerative Medicine, [b]Department of Hematology and Oncology, [c]Department of Cell Transplantation and Regenerative Medicine; Tokai University School of Medicine, Isehara, Kanagawa, Japan; [d]Molecular Medicine and Therapy, United Centers for Advanced Research and Translational Medicine, Tohoku University Graduate School of Medicine, Sendai, Miyagi, Japan; [e]Service de Nephrologie, Universite Catholique de Louvain, Brussels, Belgium

Correspondence: Takashi Yahata, Ph.D., Tokai University School of Medicine, Isehara, Kanagawa 259-1193, Japan. Telephone: 81-463-1121; Fax: 81-463-92-4750; e-mail: yahata@is.icc.u-tokai.ac.jp; or Kiyoshi Ando, M.D., Ph.D., Tokai University School of Medicine, Isehara, Kanagawa 259-1193, Japan. Telephone: 81-463-1121; Fax: 81–463-92-4750; e-mail: andok@keyaki.cc.u-tokai.ac.jp

Received August 12, 2013; accepted for publication October 3, 2013; first published online in STEM CELLS *EXPRESS* October 24, 2013.

© AlphaMed Press
1066-5099/2014/$30.00/0

http://dx.doi.org/10.1002/stem.1577

ABSTRACT

The prognosis of patients undergoing hematopoietic stem cell transplantation (HSCT) depends on the rapid recovery and sustained life-long hematopoiesis. The activation of the fibrinolytic pathway promotes hematopoietic regeneration; however, the role of plasminogen activator inhibitor-1 (PAI-1), a negative regulator of the fibrinolytic pathway, has not yet been elucidated. We herein demonstrate that bone marrow (BM) stromal cells, especially osteoblasts, produce PAI-1 in response to myeloablation, which negatively regulates the hematopoietic regeneration in the BM microenvironment. Total body irradiation in mice dramatically increased the local expression levels of fibrinolytic factors, including tissue-type plasminogen activator (tPA), plasmin, and PAI-1. Genetic disruption of the *PAI-1* gene, or pharmacological inhibition of PAI-1 activity, significantly improved the myeloablation-related mortality and promoted rapid hematopoietic recovery after HSCT through the induction of hematopoiesis-promoting factors. The ability of a PAI-1 inhibitor to enhance hematopoietic regeneration was abolished when *tPA*-deficient mice were used as recipients, thus indicating that PAI-1 represses tPA-dependent hematopoietic regeneration. The PAI-1 inhibitor not only accelerated the expansion of the donor HSCs during the early-stage of regeneration, but also supported long-term hematopoiesis. Our results indicate that the inhibition of PAI-1 activity could be a therapeutic approach to facilitate the rapid recovery and sustained hematopoiesis after HSCT. STEM CELLS *2014;32:946–958*

INTRODUCTION

Hematopoietic stem cell transplantation (HSCT) is used as a therapy for patients who suffer from hematological malignancies. In general, such patients are myeloablated by chemotherapy and/or radiotherapy to eradicate the deranged host hematopoietic system, followed by transplantation of healthy donor-derived hematopoietic cells [1]. However, due to a low engraftment efficiency and delayed bone marrow (BM) reconstitution, these patients occasionally suffer from severe immunodeficiency, thus leading to an increased susceptibility to serious infectious diseases, and therefore, to a high-risk of transplant-related death [2]. The establishment of an efficient strategy to improve the recovery and sustain hematopoiesis is a goal in the treatment of patients undergoing HSCT.

The fibrinolytic pathway breaks down fibrin clots in the blood, and plasmin plays a central role in this process [3]. The proenzyme plasminogen (Plg) is produced from the liver and circulates in the blood stream. Under certain circumstances, such as wound healing, Plg is proteolytically converted into the active enzyme plasmin by tissue-type plasminogen activator (tPA), which is released from endothelial cells [4]. The blood also contains negative regulators of the fibrinolysis pathway, including plasminogen activator inhibitor-1 (PAI-1). The production of plasmin from plasminogen is thus regulated by a balance between activator molecules (e.g., tPA) and their inhibitors (e.g., PAI-1) [4, 5]. Therefore, inhibiting the PAI-1 activity is expected to accelerate the activation of the tPA-mediated fibrinolytic pathway.

Recently, Hattori and colleagues demonstrated that the fibrinolytic pathway regulates hematopoietic regeneration [6, 7]. They showed that the deletion of the Plg gene impaired the entry of quiescent HSCs into the cell cycle and delayed hematopoietic regeneration. In contrast, the activation of Plg by the exogenous administration of recombinant tPA promoted HSC proliferation and differentiation

©AlphaMed Press 2013

through the potentiation of matrix metalloproteinase (MMP)-mediated release of c-kit ligand (c-kitL) from BM stromal cells. The fibrinolytic pathway thus plays a role in hematopoiesis.

We have recently developed a low molecular weight synthetic inhibitor of PAI-1, TM5275 (5-chloro-2[[(2-[4-(diphenylmethyl) piperazine-1yl]-2-oxoethoxy)acetyl) amino]benzoate) [8, 9]. TM5275 binds selectively to the A β-sheet (s4A) position of the PAI-1 molecule, preventing the formation of the PAI-1/tPA complex, thereby preserving active tPA. Previous studies have demonstrated that TM5275, which was given orally, provided antithrombotic benefits without prolonging the bleeding time in rodent and monkey thrombosis models [10]. Given the potential importance of the fibrinolytic pathway in HSCT, in this study, we addressed whether the suppression of PAI-1 activity could affect the hematopoietic regeneration after transplantation in PAI-1 knockout (KO) mice and using the PAI-1 inhibitor, TM5275. Our study demonstrates that PAI-1 is a negative regulator of hematopoietic regeneration, and that suppression of the PAI-1 activity leads to both a rapid recovery and long-term maintenance of donor-derived hematopoiesis. Therefore, the inhibition of PAI-1 activity could be a therapeutic approach to facilitate rapid recovery and sustained hematopoiesis.

Materials and Methods

Animals

Eight- to twelve-week-old C57Bl/6J mice were purchased from CLEA Japan (Tokyo, Japan, www.clea-japan.com). *PAI-1*-deficient mice (B6.12952-Serpine1^{tm1Mg}/J) [11, 12] were purchased from Jackson Laboratory (Bar Harbor, ME, www.jax.org). *tPA*-deficient mice (B6.129S2-Plat^{tm1Mlg}/J) [13] were kindly provided by Dr. Koichi Hattori, University of Tokyo, Japan. All mice were housed in cages at the animal facility of Tokai University School of Medicine. All the protocols for animal experiments were approved by the Animal Care Committee of Tokai University, and animals were treated in accordance with the institutional guidelines.

Cell Transplantation

To distinguish donor (Ly5.1)- and recipient (Ly5.2)-derived BM cells, we used the Ly5.1/Ly5.2 congenic system and analyzed the reconstitution of hematopoietic cells by a fluorescence-activated cell sorting (FACS) analysis by gating Ly5.1$^+$ donor-derived cells. Before transplantation, the recipient mice were lethally irradiated (9 Gy) in an x-ray irradiator (MBR-1520R-3, Hitachi Medico, Tokyo, Japan, www.hitachi-power-solution.com). Ly5.1$^+$ BM mononucleic cells (MNCs, 2.5 $\times$ 10^6) were transplanted intravenously into the retro-orbital plexus of Ly5.2$^+$ congenic mice.

For the secondary transplantation, 1 $\times$ 10^6 donor-derived Ly5.1$^+$ BM MNCs from the primary recipients were retransplanted into Ly5.2$^+$ secondary recipients which had been irradiated with 9 Gy. To protect secondary recipients from radiation-related lethality, 5 $\times$ 10^5 Ly5.2$^+$ competitor cells were transplanted along with the Ly5.1$^+$ donor cells. To compare the proportion of long-term HSCs, Ly5.1$^+$ BM cells from the primary recipients were serially diluted and administered along with 5 $\times$ 10^5 Ly5.2$^+$ competitor cells into secondary recipients that had been irradiated with 9 Gy. At 12 weeks after secondary transplantation, the BM MNCs were collected and stained with APC-conjugated anti-Ly5.1, FITC-conjugated anti-B220, PE-conjugated anti-Gr-1 and anti-Mac-1 antibodies, and were analyzed by FACS LSRFortessa (BD Bioscience, San Jose, CA, www.bdbioscience.com). The proportion of donor cells was calculated from a total of 200,000 events. Successfully engrafted mice were defined as recipients that contained more than 1.0% Ly5.1$^+$ donor-derived cells with both lymphoid (B220$^+$) and myeloid (Gr-1$^+$/Mac-1$^+$) differentiation markers. In the radioprotection assay, we used 12 Gy irradiation, which results in 20% survival when 1 $\times$ 10^6 cells were transplanted (Supporting Information Fig. S1).

Administration of the PAI-1 Inhibitor or tPA

TM5275 is a specific inhibitor of PAI-1 molecules that had a half-maximal inhibition (IC_{50}) value of 6.95 μM in a tPA-dependent hydrolysis assay [8, 10]. It does not interfere with other serpin/serine protease systems, such as the alpha1-antitrypsin/trypsin and alpha2-antiplasmin/plasmin systems.

After BM transplantation, TM5275 (100 mg/kg) or vehicle (saline) was administered daily to mice via oral gavage using a feeding needle for 5 consecutive days. Recombinant tPA (10 mg/kg, Eisai, Tokyo, Japan, www.eisai.com) was administered to the mice daily by intraperitoneal injection for 5 consecutive days. The dosage is equivalent to that used in the clinical setting.

Immunohistochemistry

Isofluorane-anesthetized mice were perfused with 4% paraformaldehyde in phosphate buffered saline (PBS) through the left ventricle. The femur and tibia were removed, decalcified, embedded in OCT compound, and frozen in liquid nitrogen. Alternatively, the decalcified bones were embedded in paraffin. The deparaffinized sections were stained for tPA by incubation with a rabbit anti-mouse tPA polyclonal antibody (Santa Cruz Biotechnology, California, CA, www.scbt.com), for Plg/plasmin with a rabbit anti-human Plg/plasmin polyclonal antibody (Santa Cruz Biotechnology) or for PAI-1 with a rabbit anti-mouse PAI-1 polyclonal antibody (Abcam, Cambridge, MA, www.abcam.com), followed by visualization with a catalyzed signal amplification II system (Dako, California, CA, www.dako.com). The slides were then developed with diaminobenzidine and counterstained with methyl green. For the double immunohistochemical staining analysis, the bone sections were stained with PAI-1 or tPA antibodies, followed by costaining with either rat anti-mouse PECAM-1 (CD31) monoclonal antibodies (BD BioSciences), goat anti-mouse osteocalcin polyclonal antibodies (Santa Cruz Biotechnology), or goat anti-mouse alpha one chain of type I collagen (Col(I) α1) polyclonal antibodies (Santa Cruz Biotechnology). Serial sections of bone were stained with rabbit anti-mouse c-kit polyclonal antibodies (Santa Cruz Biotechnology) or rabbit anti-mouse proliferation cell nuclear antigen (PCNA) polyclonal antibodies (Abcam). Fluorescent immunohistochemistry was also performed with secondary antibodies as follows: Alexa Fluor 488 goat anti-rabbit IgG, Alexa Fluor 594 donkey anti-goat IgG or Alexa Fluor 594 goat anti-rabbit IgG secondary antibody (Life Technologies Corporation, Grand Island, NY, www.lifetechnologies.com), followed by counterstaining with 4′,6-diamidino-2-phenylindole. The endosteal region of the BM was defined as that within 12 cells from the endosteum [14, 15]. Images were captured using a HS All-in-one Fluorescence Microscope Biorevo 9000 (Keyence Corporation, Osaka, Japan, www.keyence.com) and analyzed by the BZ II analyzer software program (Keyence Corporation).

©AlphaMed Press 2013

Evaluation of the tPA, Plasmin, PAI-1, MMP-9, and C-KitL Levels in Blood Plasma and BM Fluid

Plasma was prepared from peripheral blood (PB) with EDTA as an anticoagulant, and then the specimens were centrifuged at 11,600*g* for 10 minutes to completely remove platelets. BM liquid was collected as described previously [16]. Briefly, four long leg bones were perused with 1 ml of PBS containing 2 mM ethylenediaminetetraacetic acid (EDTA) and 0.5% bovine serum albumin (BSA). BM cells were removed by centrifugation at 350*g*, and the resulting supernatant was designated as BM liquid. The volume of the BM cavities of the bones was assumed to be 25 μl in this study, and the cytokines concentration were multiplied by this dilution factor (1,000/25 = 40×) and expressed per unit BM volume as described previously [16]. The concentrations of plasmin (Innovative Research, Novi, MI, www.innov-research.com), tPA (Innovative Research), active PAI-1 (Innovative Research), total MMP-9 (R&D System, MN, www.rndsystems.com), and stem cell factor (SCF) (c-kitL, R&D System) in the plasma and in BM fluid were determined by enzyme-linked immunoabsorbent assay (ELISA) kits according to the manufacturers' instructions.

PB Cell Counts

PB was collected and a complete blood count was determined using a Sysmex Hematology Analyzer (Sysmex Co., Kobe, Japan, www.sysmex.com).

Analysis of HSC and Cell Engraftment

On day 2 and 1, 3, and 15 weeks after the infusion of MNCs, the mice were euthanized, and the BM MNCs were collected from the femurs and tibiae. The BM MNCs were counted, and aliquots of cells were stained with various antibodies as noted below. Donor-derived hematopoietic cells were labeled with a PE-conjugated anti-Ly5.1 antibody (CD45.1, BD Biosciences) and biotin-conjugated antibody cocktail for lineage markers (CD5, CD11b, CD45R, Gr-1, 7-4, and Ter119; Miltenyi Biotec, Bergisch Gladbach, Germany, www.miltenyibiotec.com), followed by perinidin chlorophyll protein-cyanine 5.5 (PerCP-Cy5.5)-conjugated streptavidin (BD Biosciences). The labeled cells were divided into two aliquots, each of which was then mixed with either antibody cocktail A (APC-conjugated anti-mouse c-kit [CD117] antibody [eBioscience, San Diego, CA, www.ebioscience.com], PE-Cy7-conjugated anti-mouse Sca-1 [Ly6A/E] antibody [eBioscience], and FITC-conjugated anti-mouse CD34 antibody [eBioscience]) or with antibody cocktail B (APC-conjugated anti-mouse CD48 antibody [eBioscience] and PE-Cy7-conjugated anti-mouse CD150 antibody [eBioscience]). A flow cytometric analysis was performed on the FACS LSRFortessa (BD Bioscience) instruments using the FACS-Diva software program (BD Bioscience). Dead cells were gated out by staining with propidium iodide. The proportion of each lineage was calculated from 1,000,000 events.

Cell Proliferation and Cell Cycle Analysis

At 1 week post-transplantation, Ly5.1$^+$, lineage-negative, Sca-1-positive, c-kit-positive (LSK) cells were isolated and stained with anti-Ki67-FITC antibody according to the manufacturer's instructions (BD Bioscience).

Statistical Analysis

The data were analyzed using unpaired two-tailed Student's *t* tests or the Log-rank test for the survival analysis using the PRISM software program (GraphPad software, LA Jolla, CA, www.graphpad.com). For comparisons of more than three groups, a one-way ANOVA followed by Bonferroni post-tests was performed. A value of $p < .05$ was considered to be significant.

RESULTS

Irradiation Activates the Fibrinolytic Pathway and Increases the Expression of PAI-1 in the BM Microenvironment

To examine the effects of irradiation on the fibrinolytic system in the BM microenvironment, the levels of fibrinolytic factors, such as tPA, plasmin/Plg, and its inhibitor, PAI-1, in the BM fluid and in plasma were measured by ELISA. Two days after 9 Gy irradiation, the levels of tPA and plasmin in the BM fluid, as well as in the plasma, were significantly elevated (Fig. 1A). The level of active PAI-1, a negative regulator of the fibrinolytic system, was also elevated in the plasma and BM fluid of the irradiated mice (Fig. 1A). Of note, the increases of these fibrinolytic factors and PAI-1 were much more prominent in the BM fluid than in the blood, suggesting that the irradiation dramatically activates the fibrinolytic pathway and its inhibitor, PAI-1, in the hematopoietic microenvironment.

Increases in the expression levels of tPA, plasmin (or Plg), and PAI-1 in the BM microenvironment were also confirmed by means of immunohistochemical approaches (Fig. 1B, 1C). The irradiation severely destroyed the BM structure, which may have increased the chance of non-specific staining. Therefore, the specificity of the antibodies used in these immunostaining was verified in tPA KO mice or PAI-1 KO mice. No substantial material in the tissue was stained with the respective antibodies under the same assay conditions in these mice (Supporting Information Fig. S2).

Next, the cells responsible for producing the fibrinolytic factors and PAI-1 in the irradiated BM were identified. tPA was detected in vasculature-lining CD31$^+$ endothelial cells and was significantly elevated after irradiation (Fig. 1B, 1C and Supporting Information Fig. S3A). In agreement with previous reports [4, 5], PAI-1 was detected in megakaryocyte-like cells in untreated mice, but after irradiation, the PAI-1 producing megakaryocyte-like cells disappeared, and the PAI-1 levels in the endosteal region were increased. The tissue distributions of plasmin and Plg colocalized with that of PAI-1 after irradiation (Fig. 1B). Our subsequent double-staining studies revealed that the majority of PAI-1-expressing cells in the irradiated BM were both osteocalcin-positive and Col(I) α1-positive osteoblasts (Fig. 1C and Supporting Information Fig. S3B, S3C).

The activation of fibrinolytic factors and the fibrinolysis inhibitor, PAI-1, in nonhematopoietic cells in the hematopoietic niche shortly after irradiation was also conformed in in vitro studies. We observed that primary BM stromal cells, as well as the BM stromal cell line, HESS5, produced fibrinolytic factors and PAI-1 after irradiation (Fig. 1D and Supporting Information Fig. S4).

PAI-1 Is a Negative Regulator of Early-Phase Hematopoietic Regeneration

To investigate role of PAI-1 in the hematopoietic regeneration, we transplanted 2.5 × 10^6 Ly5.1$^+$ BM MNCs into Ly5.2$^+$

©AlphaMed Press 2013

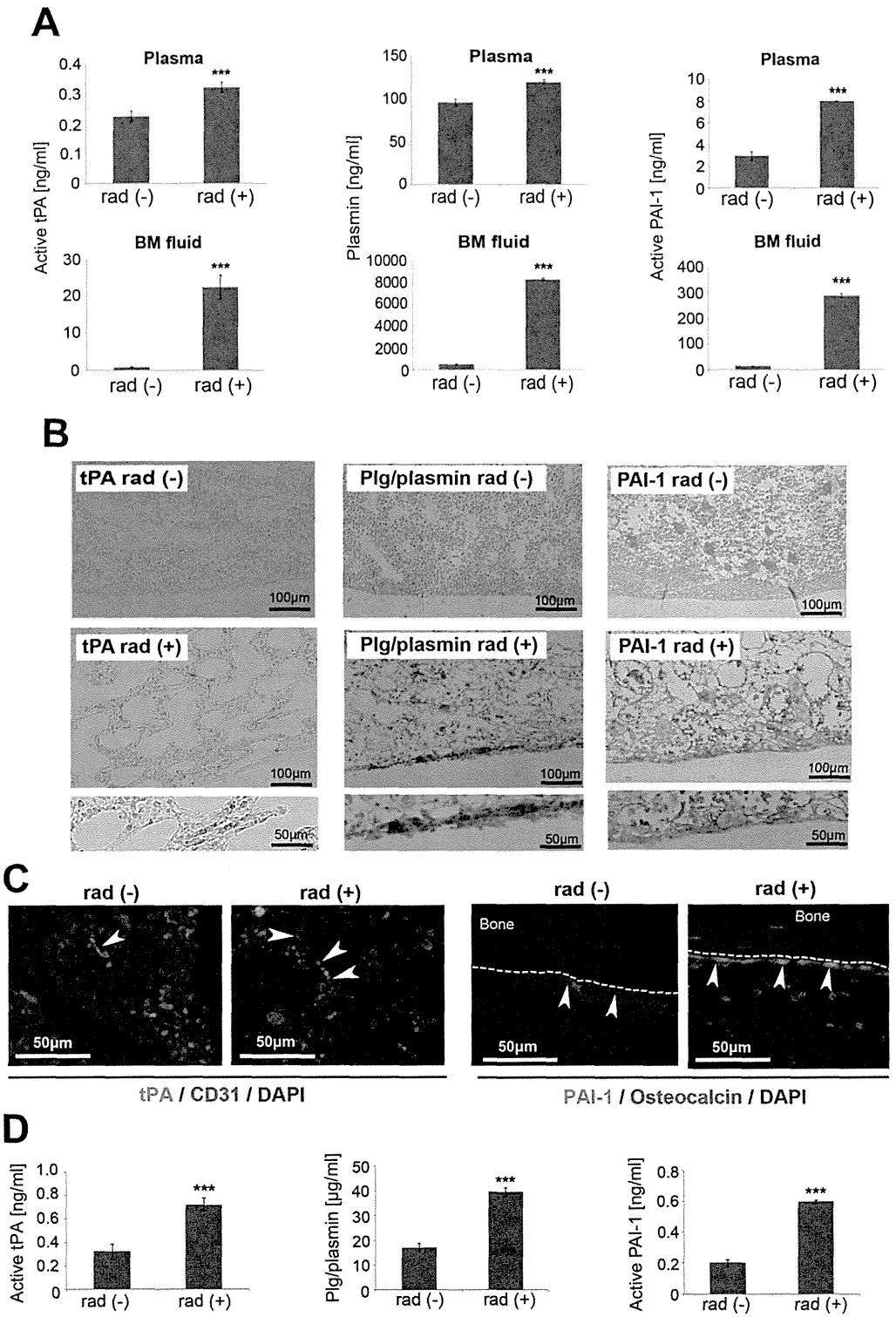

Figure 1. The fibrinolytic pathway and its inhibitor are activated after irradiation. Mice were treated with 9 Gy irradiation [rad (+)] or were untreated [rad (−)], and plasma and BM fluid were collected 2 days later. **(A):** The concentrations of active tPA, plasmin, and active PAI-1 in the plasma and BM fluid were determined by enzyme-linked immunoabsorbent assay (ELISA). Data from three independent experiments are shown ($n = 6$ for each condition; ***, $p < .001$) and are expressed as the means ± SD. **(B, C):** Representative images of immunohistochemical staining for tPA, Plg/plasmin, and PAI-1 in the femur BM. Cells at the endosteal region were intensely stained. (C): The sections were double-immunostained with antibodies for CD31 (red) and tPA (green) (left set), or osteocalcin (red) and PAI-1 (green) (right set). Nuclei were counterstained with DAPI (blue). Arrowheads indicate positive cells. **(D):** The irradiation-induced expression of fibrinolytic factors in cultured BM cells. Primary BM stromal cells in culture were exposed to 10 Gy irradiation. The culture media were collected 24 hours after irradiation, and the concentrations of active tPA, Plg/plasmin, and active PAI-1 were measured by ELISA. Data from three independent experiments are shown ($n = 6$ for each condition; ***, $p < .001$ vs. [rad (−)]) and are expressed as the means ± SD. Abbreviations: BM, bone marrow; DAPI, 4′,6-diamidino-2-phenylindole; PAI-1, plasminogen activator inhibitor-1; tPA, tissue-type plasminogen activator; Plg, plasminogen.

©AlphaMed Press 2013

congenic mice, which had been myeloablated by 9 Gy irradiation. PAI-1 KO mice (Ly5.2$^+$) were used as HSCT recipients to monitor the effects of the PAI-1 inhibition on hematopoietic regeneration. The PAI-1 KO recipient mice did not exhibit the induction of active PAI-1, regardless of the transfer of wild-type (WT; PAI-1$^{+/+}$) hematopoietic cells, suggesting that donor-derived hematopoietic cells may not be involved in the regulation of the fibrinolytic pathway during hematopoietic regeneration (Fig. 2A).

A previous study by another group [6] reported that the activation of the fibrinolytic pathway by recombinant tPA promoted hematopoietic cell proliferation through the MMP-mediated release of c-kitL. We therefore evaluated the expression levels of active tPA and other hematopoietic regulatory factors (i.e., MMP-9 and c-kitL) in the PAI-1 KO mice. The results demonstrated a marked increase in the expression of these factors compared to the WT mice at each time point (Fig. 2B–2E).

We subsequently examined the efficiency of hematopoietic regeneration by a flow cytometric analysis (Supporting Information Fig. S5). Over 90% (93.96% $\pm$ 1.56%, $n = 36$) of the hematopoietic cells in the recipient BM were Ly5.1$^+$ donor-derived cells. The absolute number of BM MNCs (Fig. 2F) and the proportion of Ly5.1$^+$ donor-derived Lin$^-$ SLAM (CD150$^+$CD48$^-$) HSCs (Fig. 2G, 2H) were higher in the PAI-1 KO mice than in the WT mice during both the steady state and post-transplant periods. We also examined another HSC marker, CD34$^-$LSK (Lin$^-$Sca-1$^+$c-kit$^+$), and showed that the proportion of Ly5.1$^+$ CD34$^-$LSK cells was higher in the PAI-1 KO mice than in the WT mice (Fig. 2I, 2J), supporting our hypothesis that the induction of PAI-1 in the hematopoietic microenvironment inhibits hematopoietic regeneration. Collectively, our results demonstrated that radiation-induced myeloablation augments the expression levels of not only hematopoietic regeneration-enhancing factors, tPA and Plg/plasmin, but also simultaneously enhances the expression of their negative regulator, PAI-1.

The Expression of Fibrinolytic Factors Is Augmented by PAI-1 Inhibition During Hematopoietic Recovery

We tested our hypothesis that the pharmacological inhibition of PAI-1 can augment the endogenous tPA-mediated fibrinolytic pathway activity more efficiently than exogenous tPA administration, leading to more efficient hematopoietic reconstitution after BM transplantation. A PAI-1 inhibitor or recombinant tPA was thus administered to the WT irradiated mice, and the early phase of hematopoietic recovery and the changes in fibrinolytic factors and the fibrinolysis inhibitor in the plasma were monitored at several time points. The administration of a PAI-1 inhibitor resulted in almost complete suppression of the elevation of active PAI-1 after BM transplantation (Fig. 3A). The PAI-1 inhibitor significantly increased the plasma levels of active tPA and plasmin (Fig. 3B, 3C). Based on the fact that the half-life of recombinant tPA is only a few minutes in rodents [17], as well as the results in Figure 1, it is likely that the increased tPA present at 2 and 7 days post-transplantation reflects the local production of tPA in the BM generated by irradiation. Surprisingly, the PAI-1 inhibitor augmented the induction of fibrinolytic factors more strongly than did the direct administration of recombinant tPA. This may be explained, at least in part, by the fact high PAI-1 activity was maintained during recombinant tPA administration (Fig. 3A), which may limit its benefit on fibrinolytic factors.

We confirmed that administering a PAI-1 inhibitor to mice induced an increase in the plasma levels of hematopoiesis-promoting factors, such as MMP-9 and c-kitL (3- and 1.7-fold compared to the vehicle treatment, respectively) as shown in Figure 3D and 3E. These results demonstrate that the inhibition of PAI-1 effectively induces factors promoting hematopoiesis.

The Activation of the Fibrinolytic Pathway by PAI-1 Inhibition Enhances the Hematopoietic Reconstitution

The protection against BM damage after irradiation and/or chemotherapy is a primary factor that determines the survival rate of animals [18], which hinges on how rapidly the transplanted (i.e., following radioablation) or remaining (i.e., following chemotherapy) hematopoietic cells can reconstitute the crippled hematopoietic system. The survival rates of recipient mice after either a lethal dose of radiation (12 Gy) or 5-fluorouracil administration were investigated in the presence of either recombinant tPA or a PAI-1 inhibitor. The administration of tPA improved the survival rate after myeloablative treatment, but PAI-1 inhibitor treatment offered significantly more effective protection (Fig. 4A, 4B).

The benefits on the hematopoietic recovery were also confirmed in 9 Gy-irradiated mice, which had been transplanted with BM MNCs. The numbers of both white blood cells and platelets markedly increased after BM transplantation: the PAI-1 inhibitor treatment led to more successful hematopoietic recovery than did the treatment with recombinant tPA (Fig. 4C, 4D). These results demonstrate that the inhibition of PAI-1 promotes hematopoietic recovery and protects against myeloablation-induced mortality.

Suppressing the PAI-1 Activity Induces tPA-Mediated HSC Proliferation in the BM After HSCT

To further elucidate the mechanism(s) by which the PAI-1 inhibition improves the hematopoietic recovery, 2.5×10^6 Ly5.1$^+$ BM cells were transplanted into the 9 Gy-irradiated Ly5.2$^+$ congenic mice, and the effects of tPA or a PAI-1 inhibitor on the proliferation of HSCs were assessed. The absolute number of BM MNCs in the recipients indeed increased in the mice given a PAI-1 inhibitor (Fig. 5A). At 3 weeks after transplantation, both the proportion and the absolute number of phenotypically identified Ly5.1$^+$ donor-derived HSC compartments were significantly higher in the PAI-1 inhibitor-treated mice than in the control or the tPA-treated mice (Fig. 5B–5E). The proportion of mature myeloid and lymphoid Ly5.1$^+$ donor-derived cells in the recipient BM was equivalent in the vehicle-treated and PAI-1 inhibitor-treated recipients, suggesting that the PAI-1 inhibitor does not influence the differentiation of HSCs (Supporting Information Fig. S6). The ability of a PAI-1 inhibitor to induce hematopoietic regeneration, that is, upregulation of MMP and c-kitL production and enhancement of donor cell engraftment was completely negated when the tPA KO mouse was used as the recipient (Fig. 5F–5J), further supporting our hypothesis that the hematopoietic regeneration in our model was derived from the

©AlphaMed Press 2013

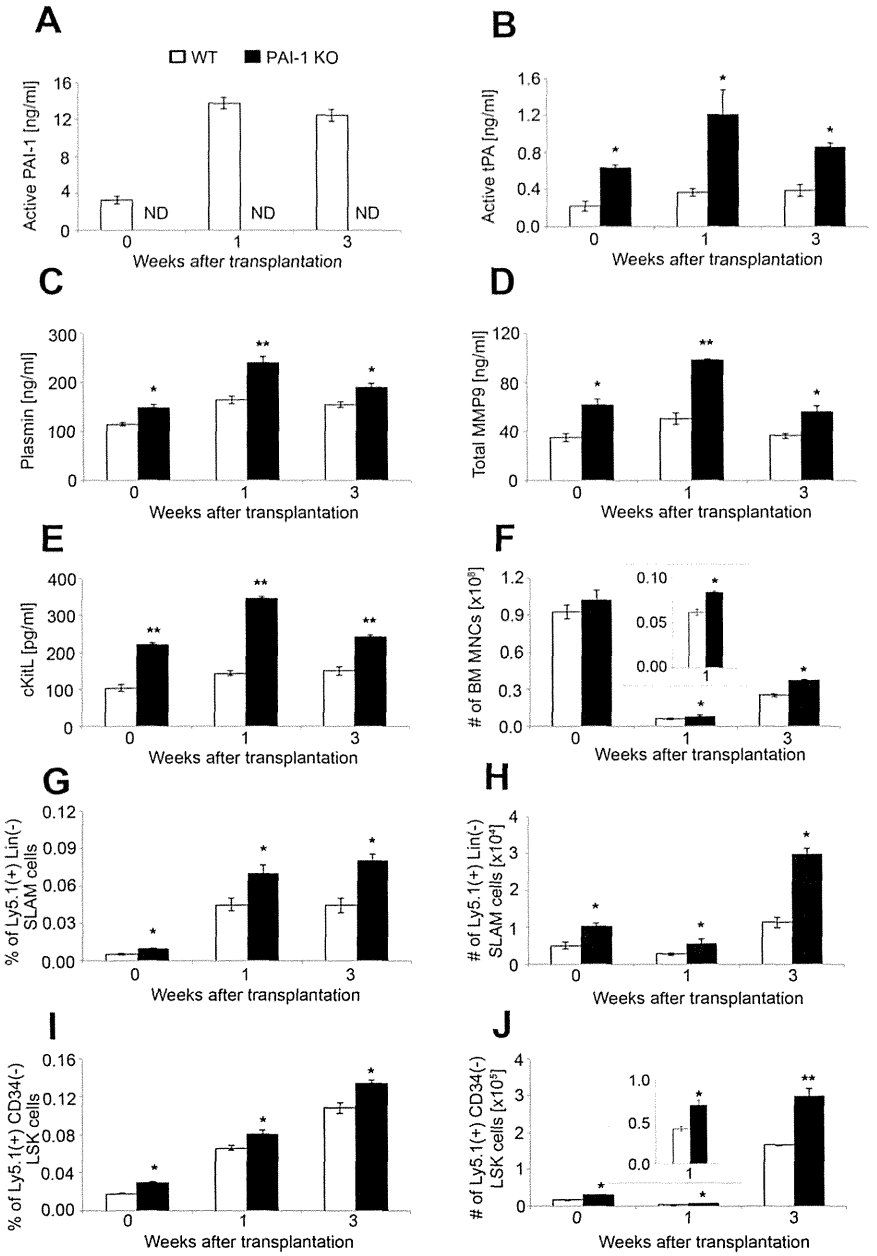

Figure 2. Hematopoietic regeneration is enhanced in PAI-1 KO mice. BM MNCs (2.5×10^6) from the Ly5.1$^+$ donor mice (PAI-1$^{+/+}$) were transplanted into WT (Ly5.2$^+$, PAI-1$^{+/+}$) or PAI-1 KO (Ly5.2$^+$, PAI-1$^{-/-}$) mice that had been irradiated with 9 Gy. Plasma was collected from the recipient mice 1 or 3 weeks after transplantation. **(A–E):** The levels of soluble factors in the plasma. The levels of active PAI-1 (A), active tPA (B), plasmin (C), total MMP-9 (D), and c-kitL (E) in the plasma were determined by enzyme-linked immunoabsorbent assay. Plasma samples from unirradiated (untransplanted) mice were used as controls (0 weeks). White and black bars represent WT and PAI-1KO recipient mice, respectively. The data from three independent experiments are shown ($n = 9$ for each condition). *, $p < .05$; **, $p < .01$ versus WT at the respective time points. ND, not detected. Data are expressed as the means ± SD. **(F–J):** BM MNCs were collected from four long leg bones (two femurs and two tibias) per mouse, pooled, and analyzed by fluorescence-activated cell sorting. The total number of BM MNCs (F), the proportion of Lin$^-$SLAM cells among the donor-derived Ly5.1$^+$ cells (G), the total number of Lin$^-$ SLAM cells (H), the proportion of CD34$^-$LSK cells among Ly5.1$^+$ cells (I), and the total number of CD34$^-$LSK cells (J) were calculated at zero, 1 and 3 weeks. The data from three independent experiments are shown ($n = 9$ for each condition). *, $p < .05$; **, $p < .01$ versus WT at the respective time points. Larger graph scales of the results at 1 week are included as inset graphs in (F) and (J). The data are expressed as the means ± SD. Abbreviations: BM, bone marrow; MNC, mononucleic cell; PAI-1, plasminogen activator inhibitor-1; tPA, tissue-type plasminogen activator; WT, wild type.

PAI-1 inhibition and subsequent tPA-mediated proliferation of HSCs during early hematopoietic reconstitution.

To confirm that the PAI-1 inhibitor induces HSC proliferation, the 9 Gy-irradiated Ly5.2$^+$ congenic mice were transplanted with 2.5×10^6 Ly5.1$^+$ BM cells and given a PAI-1 inhibitor for 5 consecutive days. The expression of Ki67 in the Ly5.1$^+$ donor-derived hematopoietic stem and progenitor cells was examined 1 week after HSCT. The Ki67$^+$ donor-derived LSK

©AlphaMed Press 2013

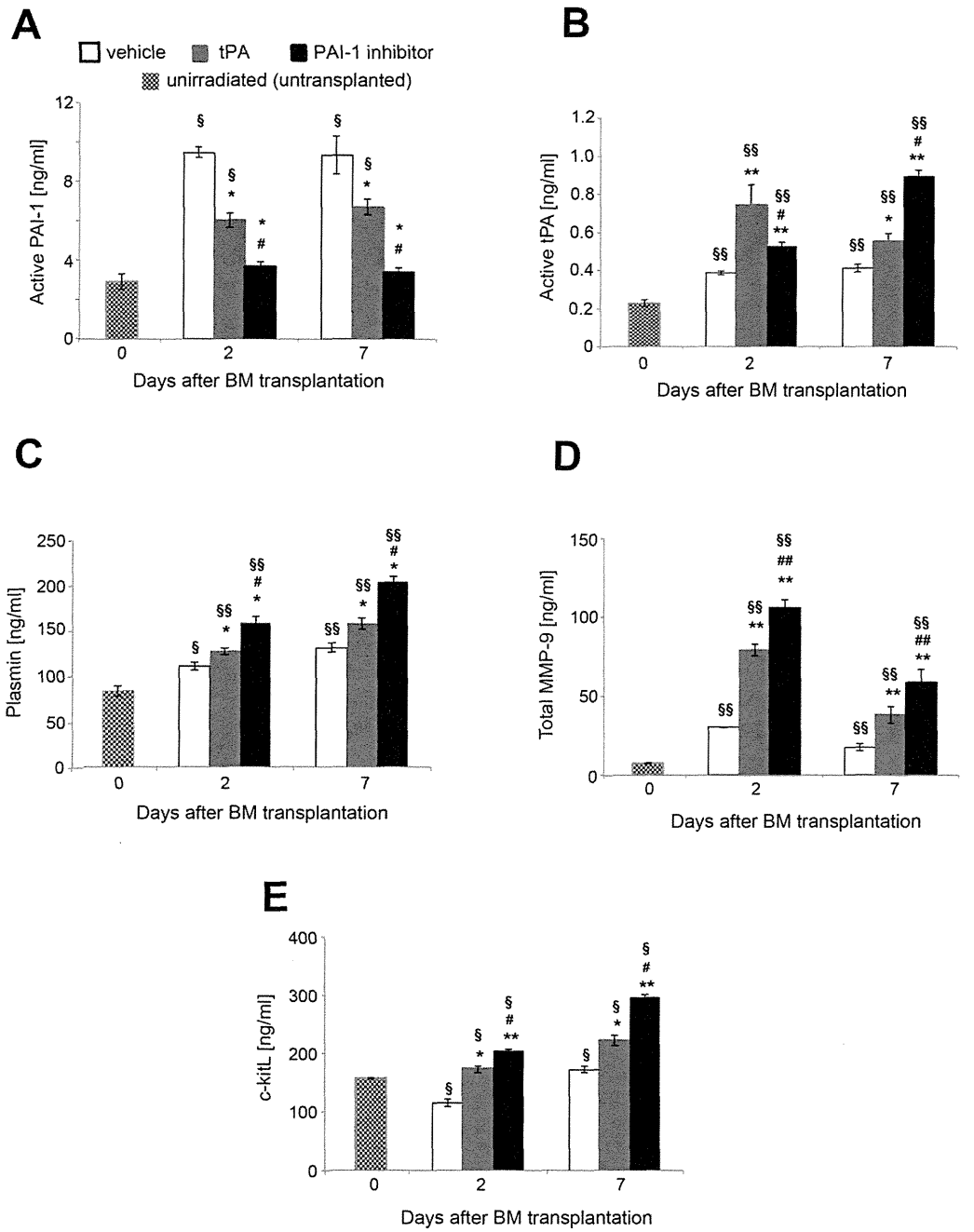

Figure 3. The PAI-1 inhibitor activates the fibrinolytic pathway during hematopoietic regeneration. BM MNCs from the Ly5.1$^+$ donor mice (2.5×10^6) were transplanted into the 9 Gy-irradiated Ly5.2$^+$ mice. Then, vehicle, tPA (10 mg/kg, i.p.), or a PAI-1 inhibitor (TM5275; 100 mg/kg, p.o.) was given daily to the recipient mice for 5 consecutive days. The plasma levels of active PAI-1 **(A)**, active tPA **(B)**, plasmin **(C)**, total MMP-9 **(D)**, and c-kitL **(E)** were measured by enzyme-linked immunoabsorbent assay. The bars in white, gray, and black represent the vehicle-, tPA-, and PAI-1 inhibitor-treated mice, respectively. Hatched bars represent the unirradiated (untransplanted) control mice. The data from four independent experiments are shown as the means ± SD ($n = 12$ for each condition). *, $p < .05$; **, $p < .01$, versus the vehicle group; #, $p < .05$; ##, $p < .01$, versus the tPA group; §, $p < .05$; §§, $p < .01$, versus the unirradiated group. Abbreviations: BM, bone marrow; PAI-1, plasminogen activator inhibitor-1; tPA, tissue-type plasminogen activator; MMP-9, matrix metalloproteinase-9.

cells were detected at the highest level in the mice given the PAI-1 inhibitor (Fig. 6A), which correlated with the HSC proportion in the recipient. The inhibition of PAI-1 thus stimulates hematopoietic stem/progenitor cells (HSPCs) to enter into the cell cycle. The PCNA$^+$c-kit$^+$ proliferating HSPCs were preferentially located in the endosteal region of the BM (arbitrarily defined as within 12 cells of the endosteum) [14, 15] at 1 week after transplantation (69.4% ± 4.1%; $n = 1{,}811$ PCNA$^+$c-kit$^+$ cells in the vehicle-treated group and 76.7% ± 3.4%; $n = 2{,}983$ PCNA$^+$c-kit$^+$ cells in the PAI-1 inhibitor-treated group, $p < .01$), indicating that the proliferation of HSPCs in the PAI-1 inhibitor-treated recipients as regulated by their interaction with the niche (Fig. 6C).

In the early-stage of regeneration, the HSPCs underwent apoptosis at a higher rate in the vehicle-treated recipient,

©AlphaMed Press 2013

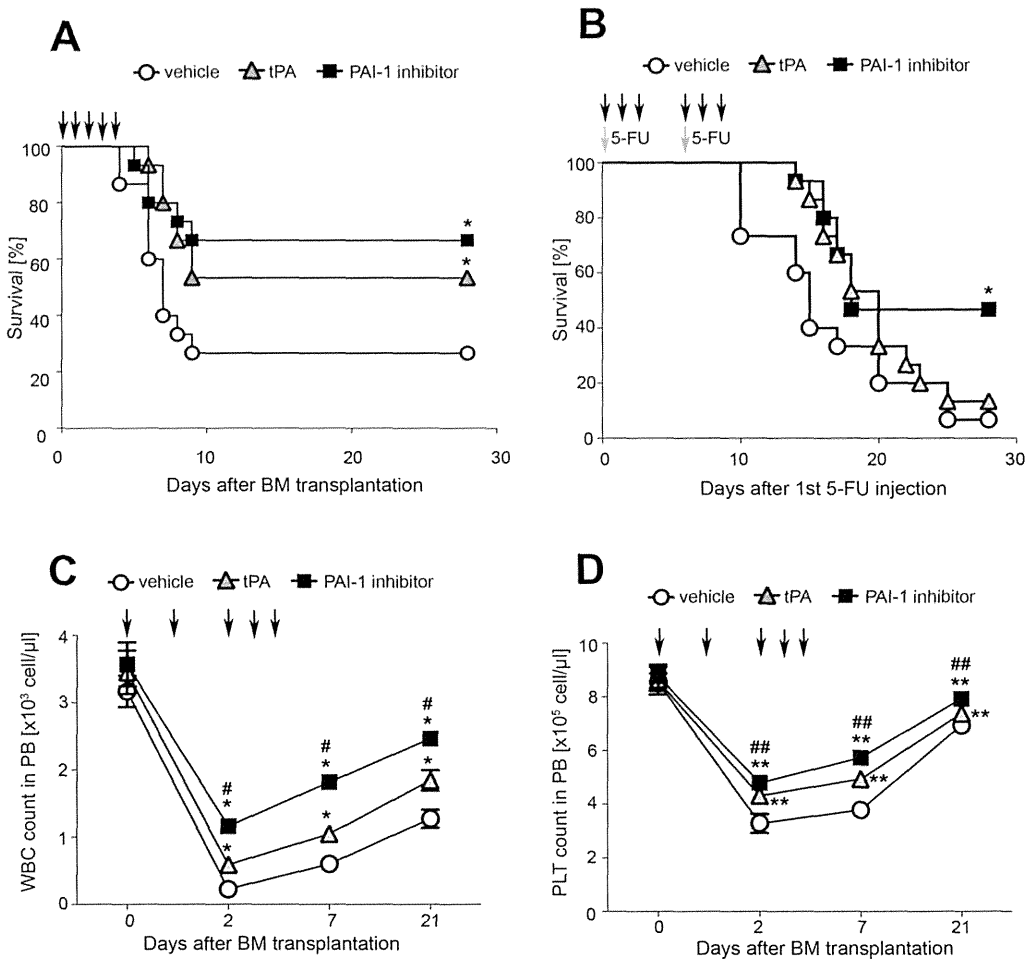

Figure 4. The PAI-1 inhibitor enhances the protection against myeloablation and promotes the rapid recovery of hematopoiesis. **(A):** The survival rate of mice after lethal-dose irradiation. Mice were exposed to 12 Gy of radiation and were transplanted with 1×10^6 BM MNCs. The mice were administered vehicle (white circle), tPA (10 mg/kg, i.p.; gray triangle), or a PAI-1 inhibitor (100 mg/kg, p.o.; black square) daily for 5 consecutive days (arrows). The data from three independent experiments are shown ($n = 15$ for each condition; *, $p < .05$ vs. the vehicle group). **(B):** The survival rate after 5-FU injection. The 5-FU (225 mg/kg, i.p.) was given twice (on days 0 and 7). The mice subsequently received vehicle (white circle), tPA (10 mg/kg, i.p.; gray triangle), or a PAI-1 inhibitor (100 mg/kg, p.o.; black square) for 3 consecutive days after the day of 5-FU injection (arrows). The data from three independent experiments are shown ($n = 15$ for each condition; *, $p < .05$ vs. both the vehicle group and the tPA group). **(C, D):** The hematopoietic recovery. Mice ($Ly5.2^+$) were exposed to 9 Gy of radiation and transplanted with 2.5×10^6 BM MNCs ($Ly5.1^+$). The numbers of white blood cells (WBC, C) and platelets (PLT, D) at the indicated time points were measured. The data from three independent experiments are shown as the means ± SD ($n = 6$ for each condition). *, $p < .05$; **, $p < .01$ versus the vehicle group, #, $p < .05$; ##, $p < .01$ versus the tPA group. Abbreviations: BM, bone marrow; PB, peripheral blood; PAI-1, plasminogen activator inhibitor-1; tPA, tissue-type plasminogen activator; 5-FU, 5-fluorouracil.

whereas the PAI-1 inhibitor prevented the apoptotic cell death of HSPCs (Supporting Information Fig. S7). Altogether, these findings indicate that the PAI-1 inhibitor enhances the proliferation of HSPCs and protects them from stress-induced apoptosis, leading to improve the hematopoietic regeneration.

PAI-1 Inhibition Potentiates the Self-Renewal Capacity of HSCs

The rapid proliferation of HSCs occasionally results in their exhaustion (i.e., loss of competence as HSCs), eventually leading to the failure of long-lasting hematopoiesis in the BM [19–21]. To examine whether the elevation of tPA activity, either by tPA- or PAI-1 inhibitor administration, induced transplanted HSCs to undergo exhaustion, the recipient BM was analyzed at 15 weeks in the $Ly5.2^+$ mice that had been transplanted with $Ly5.1^+$ donor BM cells and given a PAI-1 inhibitor. The results indicated that when the PAI-1 inhibitor was administered to mice, it increased not only the number of BM MNCs (Fig. 7A), but also the proportion, as well as the absolute number of phenotypic $Ly5.1^+$ HSCs compared to the vehicle- or recombinant tPA-treated group (Fig. 7B-7E), suggesting that the inhibition of PAI-1 activity by the PAI-1 inhibitor efficiently prolonged the survival of donor-derived HSCs in the BM.

The self-renewal capacity of HSCs was also examined in a secondary transplant performed 15 weeks after the primary transplant. Twelve weeks after the secondary transplant, the chimerism of the primary donor-derived $Ly5.1^+$ hematopoietic cells was fourfold higher in the PAI-1 inhibitor-treated group than

©AlphaMed Press 2013

in the vehicle group (Fig. 7F). The inhibition of PAI-1 therefore enhances not only the rapid hematopoietic recovery in the early phase, but also the long-term self-renewal capacity of HSCs.

To compare the repopulating activity of long-term HSCs, a small number of primary Ly5.1$^+$ donor-derived hematopoietic cells after limiting dilution was transplanted into Ly5.2$^+$ mice (6×10^4 or 2×10^4 cells per mouse). Recipient Ly5.2$^+$ mice were thought to be successfully engrafted if Ly5.1$^+$ cells with the potential for multilineage differentiation were detected in excess of 1% of the total BM cells in the recipient (representative FACS profiles are shown in Supporting Information Fig. S8). The results demonstrated that the chimerism of Ly5.1$^+$ cells was higher in the PAI-1 inhibitor-treated group (1.26% ± 0.1% with 2×10^4 cells and 3.45% ± 1.09% with 6×10^4 cells) than in the vehicle-treated group (0.38% ± 0.26% with 2×10^4 cells and 1.04% ± 0.19% with 6×10^4 cells) (Fig. 7G). In addition, successful engraftment was achieved more often in the PAI-1 inhibitor-treated group (five of the five mice with 2×10^4 and 6×10^4 cells) than in the vehicle-treated group (one of the five mice with 2×10^4 cells and two of the five mice with 6 $\times 10^4$ cells). Collectively, our results of the phenotypic (i.e., cell surface analysis) and repopulating (i.e., transplantation) assays revealed that inhibiting the PAI-1 activity during the early phase of reconstitution efficiently expands the long-term repopulating HSCs.

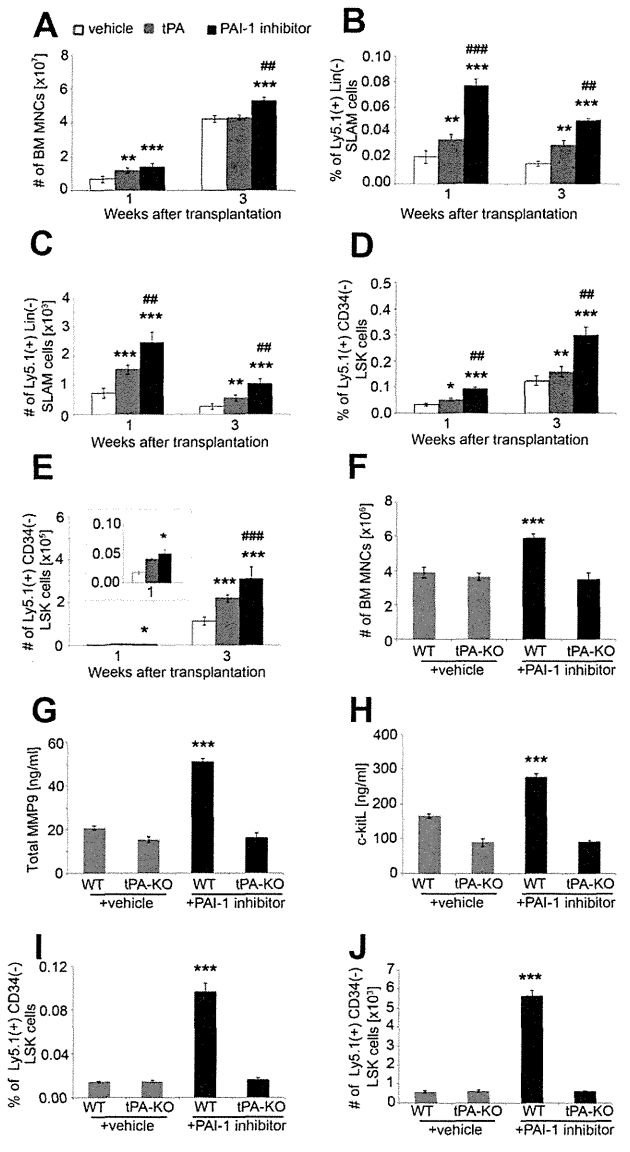

Discussion

This study was undertaken to elucidate the role of PAI-1, a negative regulator of the fibrinolytic pathway, in hematopoietic regeneration after irradiation-induced myeloablation. The results demonstrated the following: first, the expression levels of fibrinolytic factors, such as tPA and plasmin, are markedly augmented in endothelial and nonhematopoietic stromal cells, respectively, in the BM of mice after sublethal irradiation. Second, the PAI-1 expression is simultaneously upregulated in nonhematopoietic stromal cells, especially osteoblasts. Third, PAI-1 negatively regulates hematopoietic regeneration: the genetic deletion of PAI-1, as well as the administration of a PAI-1 inhibitor, activates the tPA-mediated fibrinolytic pathway, eventually accelerating hematopoietic regeneration. Finally, the inhibition of PAI-1 activity at an early phase of transplantation facilitates the recovery and maintenance of hematopoiesis (Supporting Information Fig. S9).

Previous studies have shown that the levels of fibrinolytic factors and their inhibitors are elevated in several tissues

Figure 5. The PAI-1 inhibitor increases the proportion of hematopoietic stem cells (HSCs) during hematopoietic reconstitution. BM MNCs from the Ly5.1$^+$ donor mice (2.5×10^6) were transplanted into the 9 Gy-irradiated Ly5.2$^+$ mice, followed by repeated administration of saline (vehicle), tPA (10 mg/kg, i.p.), or the PAI-1 inhibitor (100 mg/kg, p.o.) for 5 consecutive days. **(A–E):** The results of the fluorescence-activated cell sorting (FACS) analysis of the HSCs in recipient mice. BM MNCs were obtained at the indicated time points from four long leg bones per mouse, and were pooled and subjected to a FACS analysis. (A): The total number of BM MNCs per recipient. (B): The proportion of Lin$^-$ SLAM cells among the donor-derived Ly5.1$^+$ cells, (C) the total number of Lin$^-$SLAM cells, (D) the proportion of CD34$^-$LSK cells among the donor-derived Ly5.1$^+$ cells, and (E) the total number of CD34$^-$LSK cells were calculated at 1 and 3 weeks. The bars in white, gray, and black represent the vehicle-, tPA-, and PAI-1 inhibitor-treated mice, respectively. The data from four independent experiments are expressed as the means ± SD ($n = 12$ for each condition). The inset graph in (E) is a magnification of the data at 1 week. *, $p < .05$; **, $p < .01$; ***, $p < .001$ versus the vehicle group, ##, $p < .01$; ###, $p < .001$ versus the tPA group. **(F–J):** In separate experiments, WT (Ly5.2$^+$, tPA$^{+/+}$) or tPA-KO (Ly5.2$^+$, tPA$^{-/-}$) mice were exposed to 9 Gy radiation and transplanted with 2.5×10^6 BM MNCs (Ly5.1$^+$, tPA$^{+/+}$). Either vehicle or a PAI-1 inhibitor was administered to the recipient mice daily for 5 consecutive days beginning the day after the BM infusion. Plasma and BM MNCs were collected 1 week after transplantation. (F): The total number of isolated BM MNCs per mouse at the indicated time points. The plasma levels of total MMP-9 (G) and c-kitL (H) in the recipient mice. Donor-derived Ly5.1$^+$ cells were gated, and the proportion of CD34$^-$LSK cells (I) and the total number of CD34$^-$LSK cells (J) in the recipient BM were analyzed. The data from three independent experiments are shown as the means ± SD ($n = 6$ for each condition). ***, $p < .001$ by one-way ANOVA. Abbreviations: BM, bone marrow; MNC, mononucleic cell; PAI-1, plasminogen activator inhibitor-1; tPA, tissue-type plasminogen activator; WT, wild type; MMP9, matrix metalloproteinase 9.

©AlphaMed Press 2013

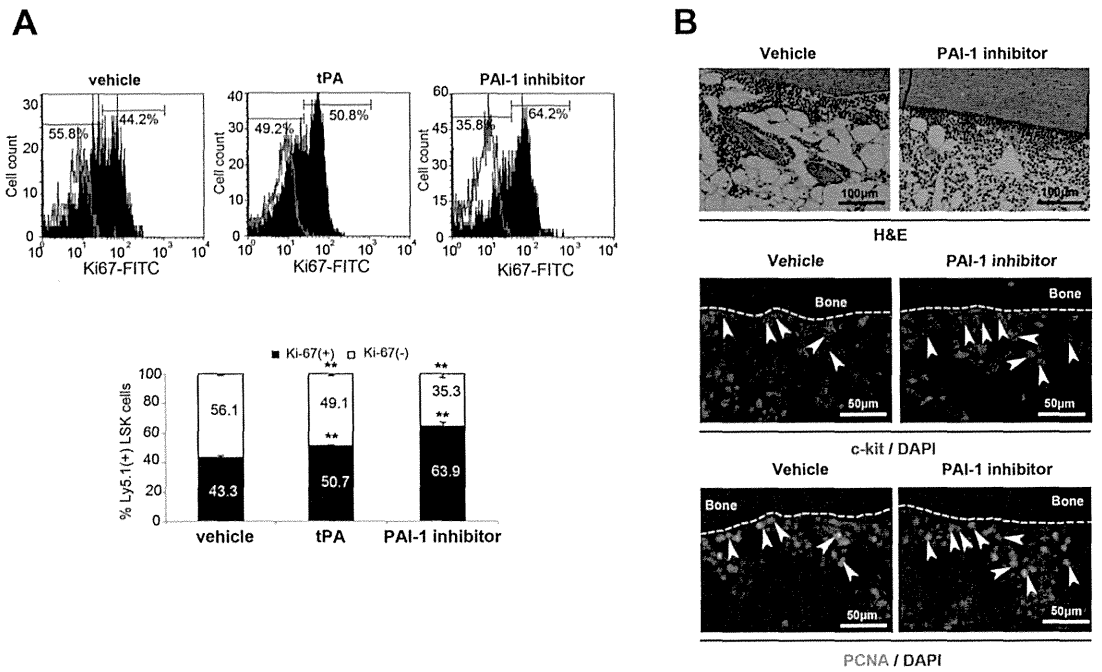

Figure 6. The PAI-1 inhibitor promotes hematopoietic stem cell (HSC) proliferation. Ly5.2$^+$ mice were exposed to 9 Gy radiation and transplanted with 2.5 × 10^6 Ly5.1$^+$ BM MNCs. Thereafter, vehicle or the PAI-1 inhibitor was administered daily to the mice for 5 consecutive days, and the mice were sacrificed on day 7 for the fluorescence-activated cell sorting (FACS) and BM histological analyses. **(A):** Representative FACS profiles of the Ki67-expression in the donor-derived Ly5.1$^+$ LSK cells. BM MNCs were collected, and the proportion of Ki67$^+$ cells among the Ly5.1$^+$ donor-derived HSCs was analyzed. Isotype-matched control IgG was used to identify the Ki67$^-$ cells. The proportion of Ki67$^+$ or Ki67$^-$ cells is shown above each histogram. The average proportion of Ki67$^+$ Ly5.1$^+$ LSK cells from three independent experiments (each with two mice) is shown in the right panel. **, $p < .01$ versus the vehicle group by one-way ANOVA followed by Bonferroni post-test. **(B):** Representative H&E staining (left panel set) or fluorescent immunostaining (c-kit [red] in the middle panel set; PCNA [green] in the right panel set) of serial sections of bone. Nuclei were counterstained with DAPI (blue). Arrowheads indicate positive cells. Abbreviations: FITC, fluorescein isothiocyanate; DAPI, 4′,6-diamidino-2-phenylindole; PAI-1, plasminogen activator inhibitor-1; H&E, hematoxylin and eosin; PCNA, proliferation cell nuclear antigen; tPA, tissue-type plasminogen activator.

following irradiation [22–24]. However, the dynamics of fibrinolytic system factors, particularly PAI-1, in hematopoietic regeneration of the BM have not been elucidated. This study revealed, for the first time, that irradiation has a substantial impact on the fibrinolytic system in the BM. Upon irradiation, the levels of fibrinolytic factors and PAI-1 in the BM fluid increased dramatically (~30-fold), in sharp contrast to the moderate increase in these factors in the plasma (1.8–3-fold). Of note, their levels in the BM fluid were 1 or 2 orders of magnitude higher than those in the plasma (e.g., 300 and 8 ng/ml of PAI-1 in the BM fluid and plasma, respectively), demonstrating that BM cells have a potent capacity to produce fibrinolytic factors and PAI-1 upon irradiation. In good agreement with these in vivo results, the results of the in vitro cultured cell experiments demonstrated that nonhematopoietic BM stromal cells readily produce tPA, plasmin, and PAI-1 after irradiation.

On closer inspection by immunohistochemistry, we identified nonhematopoietic cells, especially stromal cells, as the primary source of fibrinolytic factors and PAI-1. Our data in the irradiated PAI-1 KO mice (recipient), which have undetectable levels of PAI-1 in the plasma after transplantation of normal hematopoietic cells (PAI-1$^{+/+}$), suggested that the marked increase in PAI-1 after irradiation does not originate from donor hematopoietic cells. Nonhematopoietic stromal cells in the BM thus play a significant role in repairing the myeloablated hematopoietic microenvironment. This is not surprising, because the irradiation of mice with a lethal dose of radiation eradicates the hematopoietic cells and their progenitor cells, but not nonhematopoietic cells [25, 26].

We also elucidated the mechanism by which PAI-1 regulates the hematopoietic regeneration in the BM. A previous study by Hattori and colleagues demonstrated that activation of the fibrinolytic pathway by administration of recombinant tPA results in the conversion of the transmembrane form to the soluble form of c-kitL [6], a hematopoiesis-promoting factor. They suggested that activated plasmin subsequently transforms MMP-2/9 into active forms, which in turn release c-kitL from stromal cells. It is therefore likely that PAI-1 activity prevents the hematopoietic regeneration in the BM by inhibiting the fibrinolytic pathway and c-kitL release. Our results showing that the suppression of PAI-1 activity either by a pharmacological approach or by the genetic deletion of the PAI-1 gene can elevate the tPA/plasmin activity, promote c-kitL production, and lead to the rapid recovery of hematopoiesis after myeloablation. Although other products of fibrinolytic degradation may also promote engraftment, these results support the critical role of c-kitL production in the improvement of engraftment by PAI-1 inhibition.

Emerging evidence suggests that PAI-1 expression generally limits tissue repair by negatively regulating the fibrinolytic environment and by inhibiting cell migration [27]. For example, the skin wound healing process is accelerated in PAI-1-deficient mice [28]. PAI-1 KO mice are also protected against liver fibrosis [29] and radiation enteropathy [24]. In terms of tissue

 ©AlphaMed Press 2013